1 **Carbon export fluxes and export efficiency in the central Arctic during the**

2 **record sea-ice minimum in 2012: a joint ^{234}Th/^{238}U and ^{210}Po/^{210}Pb study**

3 **Montserrat Roca-Martí[1], Viena Puigcorbé[1,2], Michiel M. Rutgers van der Loeff[3], Christian**

4 **Katlein[3], Mar Fernández-Méndez[3,4], Ilka Peeken[3,5], Pere Masqué[1,2,6]**

5 [1]Institut de Ciència i Tecnologia Ambientals & Departament de Física, Universitat Autònoma de
6 Barcelona, 08193 Bellaterra, Spain

7 [2]School of Science and Centre for Marine Ecosystems Research, Edith Cowan University,
8 Joondalup WA 6027, Australia

9 [3]Alfred Wegener Institute for Polar and Marine Research, 27570 Bremerhaven, Germany

10 [4]Norwegian Polar Institute, Fram Centre, 9296 Tromsø, Norway

11 [5]MARUM - Center for Marine Environmental Sciences, University of Bremen, 28359 Bremen,
12 Germany

13 [6]Oceans Institute and School of Physics, The University of Western Australia, Crawley WA
14 6009, Australia

15 Corresponding authors: Montserrat Roca-Martí (Montserrat.Roca.Marti@uab.cat), Pere Masqué

16 (Pere.Masque@uab.cat)

17 **Key Points:**

18 • First use of ^{234}Th/^{238}U together with ^{210}Po/^{210}Pb as proxies for particulate organic carbon
19 export in the Arctic

20 • Low particulate organic carbon fluxes escaping from the euphotic zone during the record
21 sea-ice minimum in 2012

22 • High export efficiency of the biological pump in the central Arctic

Abstract

The Arctic sea-ice extent reached a record minimum in September 2012. Sea-ice decline increases the absorption of solar energy in the Arctic Ocean, affecting primary production and the plankton community. How this will modulate the sinking of particulate organic carbon (POC) from the ocean surface remains a key question. We use the ^{234}Th/^{238}U and ^{210}Po/^{210}Pb radionuclide pairs to estimate the magnitude of the POC export fluxes in the upper ocean of the central Arctic in summer 2012, covering time scales from weeks to months. The ^{234}Th/^{238}U proxy reveals that POC fluxes at the base of the euphotic zone were very low (2 ± 2 mmol C m^{-2} d^{-1}) in late summer. Relationships obtained between the ^{234}Th export fluxes and the phytoplankton community suggest that prasinophytes contributed significantly to downward fluxes, likely via incorporation into sea-ice algal aggregates and zooplankton-derived material. The magnitude of the depletion of ^{210}Po in the upper water column over the entire study area indicates that particle export fluxes were higher before July/August than later in the season. ^{210}Po fluxes and ^{210}Po-derived POC fluxes correlated positively with sea-ice concentration, showing that particle sinking was greater under heavy sea-ice conditions than under partially ice covered regions. Although the POC fluxes were low, a large fraction of primary production (>30%) was exported at the base of the euphotic zone in most of the study area during summer 2012, indicating a high export efficiency of the biological pump in the central Arctic.

1 Introduction

Climate change is triggering an unprecedented decline in Arctic sea ice. In September 2012 the sea-ice cover amounted to less than half of its 1979-2000 baseline [*Overland and Wang*, 2013]. Such a decrease in ice extent and thickness [*Haas et al.*, 2008] allows more sunlight to be transmitted through the sea ice, increasing the absorption of solar energy in the Arctic Ocean [*Nicolaus et al.*, 2012] and affecting sea-ice and upper-ocean ecosystems [*Wassmann*, 2011]. Net primary production (NPP) increased by 30% between 1998 and 2012 according to a satellite-based study [*Arrigo and van Dijken*, 2015]. Yet this kind of approach does not take into account the productivity of either under-ice phytoplankton nor sea-ice algae, even though it can be substantial [*Gosselin et al.*, 1997; *Fortier et al.*, 2002; *Lee et al.*, 2010; *Arrigo et al.*, 2012; *Fernández-Méndez et al.*, 2015]. However, light-driven increments in NPP will be constrained if nutrient supply to surface waters do not increase considerably by mixing or

53   upwelling [e.g. *Tremblay et al.*, 2015]. Besides this, enhanced NPP does not necessarily mean

54   larger export fluxes of particulate organic carbon (POC) to the deep ocean, since the changing

55   Arctic scenario favors a phytoplankton community structure based on the smallest cells [*Li et al.*,

56   2009]. Overall, it remains uncertain how the changes in NPP and plankton community will affect

57   the sinking of POC from the ocean surface, and in turn contribute to the marine sequestration of

58   CO_2 [*Honjo et al.*, 2010; *Anderson and Macdonald*, 2015].

59   To date, the Arctic Ocean is considered a weak sink for atmospheric CO_2, accounting for

60   ~6% of the global oceanic uptake [*Gruber et al.*, 2009]. An essential component of the ocean

61   carbon sink is the "biological pump" driven by the export of organic particles from the ocean

62   surface to its interior [*Falkowski et al.*, 1998]. During the productive season, the surface

63   downward fluxes of POC are widely heterogeneous in the Arctic, reaching higher values (>30

64   mmol C m^{-2} d^{-1}) over the shelves [e.g. *Cochran et al.*, 1995b; *Lepore et al.*, 2007] in comparison

65   to the central Arctic (<5 mmol C m^{-2} d^{-1}) [e.g. *Moran et al.*, 1997; *Cai et al.*, 2010]. However, in

66   summer 2012, a widespread deposition of ice algal biomass on the seafloor (>3000 m, median

67   estimate of 750 mmol C m^{-2}) was observed in the central Arctic associated with rapid ice melt

68   [*Boetius et al.*, 2013].

69   The export efficiency is defined as the ratio between export and production, which

70   indicates the strength of the biological pump [*Buesseler and Boyd*, 2009]. A recent model study

71   reports a high annual mean export efficiency of >30% in Arctic waters [*Henson et al.*, 2015].

72   Nevertheless, primary production and export data are very scarce, especially in the interior

73   basins [*Gustafsson and Andersson*, 2012; *Matrai et al.*, 2013]. Indeed, the temporal mismatch

74   between the measurement of production and export, combined with the existence of a long lag

75   period between both processes in the Arctic (30-40 days), make the assessment of the export

76   efficiency on a seasonal scale difficult [*Henson et al.*, 2015].

77   The radionuclide pairs ^{234}Th/^{238}U and, to a lesser extent, ^{210}Po/^{210}Pb have been used as

78   proxies of POC export since the 90s [*Buesseler et al.*, 1992; *Shimmield et al.*, 1995], but very

79   few studies have used both pairs together [*Verdeny et al.*, 2009; *Stewart et al.*, 2011; *Wei et al.*,

80   2011; *Le Moigne et al.*, 2013a]. Several authors have recommended the simultaneous use of

81   ^{234}Th/^{238}U and ^{210}Po/^{210}Pb since they cover different time scales, from weeks to months,

82   respectively, and ^{234}Th and ^{210}Po have different biogeochemical behaviors, providing

83 complementary information on POC export fluxes [*Friedrich and Rutgers van der Loeff*, 2002;
84 *Verdeny et al.*, 2009; *Stewart et al.*, 2011].

85   In this study, we aim to estimate the magnitude of the POC fluxes at the bottom of the
86 euphotic zone and within the upper mesopelagic layer in the central Arctic during the record sea-
87 ice minimum in 2012, as well as identify mechanisms that control particle export by means of
88 ^{234}Th/^{238}U and ^{210}Po/^{210}Pb. The use of both pairs may shed light on the apparent mismatch
89 between the low ^{234}Th-based export production estimates [*Cai et al.*, 2010] and the benthic
90 observations of massive sea-ice algae deposits [*Boetius et al.*, 2013] in the central Arctic. It
91 might also give a hint of the trend that POC fluxes may follow as the sea ice continues to decline.
92 To this purpose we:

93 1)   Quantify the POC export fluxes at the bottom of the euphotic zone, 50, 100 and 150 m on
94 short-term and seasonal scales by using the ^{234}Th/^{238}U and ^{210}Po/^{210}Pb pairs.

95 2)   Identify potential relationships between sea-ice conditions, phytoplankton community
96 and particle export.

97 3)   Assess the export efficiency combining the export estimates at the bottom of the euphotic
98 zone with daily, weekly and annual NPP estimates.

99 **2 Materials and Methods**

100   2.1 Study area

101   The sampling was performed from 11 August to 28 September 2012 during the ARK-
102 XXVII/3 expedition in the Eurasian Basin of the central Arctic (2 August-8 October, 2012; R/V
103 Polarstern; *Boetius* [2013]). The survey coincided with a new record low of sea-ice cover since
104 the beginning of satellite imagery in 1978 [*Parkinson and Comiso*, 2013]. The specific locations
105 and dates of the sea-ice stations are given in Figure 1 and Table 1.

106   2.2 Total ^{234}Th/^{238}U and ^{210}Po/^{210}Pb

107   Total ^{234}Th, ^{210}Po and ^{210}Pb activities were determined from seawater samples collected
108 using Niskin bottles attached to a CTD rosette. 12-depth vertical profiles from 10 to 400 m were
109 taken, with the highest resolution in the upper 150 m of the water column.

110   Total ^{234}Th activities were determined from 4 L of seawater at nine stations. Additionally,

111   replicates of deep samples (1500-3000 m) were collected for calibration purposes [*Rutgers van*

112   *der Loeff et al.*, 2006]. The samples were processed following the MnO_2 co-precipitation

113   technique [*Buesseler et al.*, 2001] using ^{230}Th as a chemical yield tracer [*Pike et al.*, 2005].

114   Briefly, the precipitates were filtered through QMA quartz fiber filters, dried overnight at 50 ºC

115   and prepared for beta counting. The counting was done on board using low background beta

116   counters (Risø National Laboratories, Denmark). Samples were re-measured after seven months

117   to quantify background activities. ^{230}Th recoveries were determined in all filters by inductively

118   coupled plasma mass spectrometry (ICP-MS) as described in *Roca-Martí et al.* [2016]. The

119   average chemical recovery was 94 ± 4% (n = 107). The parent ^{238}U activity was derived from

120   salinity using the relationship given by *Owens et al.* [2011]. Stations 4, 5 and 6 had salinities of

121   30.0-32.5 from 10 to 30 m (n = 15), falling below the range used by *Owens et al.* [2011]. For

122   these samples, we also applied the U-salinity relationship given by *Not et al.* [2012] determined

123   from sea ice, surface seawater and sea-ice brine samples, covering a wide salinity range (0-135).

124   A difference of only 1.1% in ^{238}U activity, which is lower than its associated uncertainty (1.9-

125   2.3%), was obtained using the two relationships, validating the use of Owens's relationship in the

126   present study. The ^{234}Th activity uncertainties were always ≤6%, which include those

127   uncertainties associated with counting, detector background and calibration, and ICP-MS

128   measurements.

129   Total ^{210}Po and ^{210}Pb activities were determined from 11 L of seawater at seven stations

130   using the cobalt-ammonium pyrrolidine dithiocarbamate (Co-APDC) co-precipitation technique

131   [*Fleer and Bacon*, 1984]. Samples were immediately acidified after collection with HCl to pH <2

132   and spiked with stable Pb and ^{209}Po as chemical yield tracers. Cobalt nitrate and APDC solutions

133   were added after at least one day of isotope equilibration. Samples were filtered through 0.2 µm

134   membrane filters and stored for later processing at the home laboratory. The filters were digested

135   using concentrated HNO_3 and samples were reconstructed with 1 M HCl. ^{210}Po and ^{210}Pb were

136   separated by auto-deposition of polonium onto silver discs during six hours [*Flynn*, 1968]. The

137   silver discs were then counted by alpha spectrometry using passivated implanted planar silicon

138   (PIPS) alpha detectors (Canberra, USA) and silicon surface barrier (SSB) alpha detectors

139   (EG&G Ortec, USA). Solutions were re-plated and passed through an anion exchange resin (AG

140   1-X8) to ensure the complete elimination of polonium from samples [*Rigaud et al.*, 2013].

141   Samples were re-spiked with ^{209}Po and stored for 9-11 months for later determination of ^{210}Pb

142 via ^{210}Po ingrowth. At that time samples were plated and counted once more by alpha

143 spectrometry. ^{210}Pb and ^{210}Po activities at sampling time were calculated applying in-growth,

144 decay and recovery corrections following *Rigaud et al.* [2013]. Two aliquots from each sample

145 were taken before the first and last platings to determine the chemical recovery of stable Pb by

146 inductively coupled plasma optical emission spectrometry (ICP-OES). The average recovery was

147 $87 \pm 9\%$ (n = 83). The activity uncertainties were on average 7% for ^{210}Pb and 16% for ^{210}Po,

148 which include those uncertainties associated with counting, detector background and ^{209}Po

149 activity. The larger uncertainties of ^{210}Po are due to the time elapsed between sampling and the

150 first Po plating (>80 days). All data of total ^{234}Th, ^{238}U, ^{210}Po and ^{210}Pb activities are available at

151 http://doi.pangaea.de/10.1594/PANGAEA.858790.

152   2.3 Particulate fraction

153   Large (>53 µm) particles for analyses of ^{234}Th, ^{210}Po, ^{210}Pb, POC and particulate organic

154 nitrogen (PON) were collected using in situ pumps (ISP, Challenger Oceanic, UK). Four ISP

155 were deployed at each station at 25, 50, 100 and 150 m, filtering on average 1500 L. Particles

156 were retained using 53-µm pore size nylon mesh screens and rinsed with filtered seawater. After

157 homogenization the sample was subdivided into two aliquots: one was filtered through pre-

158 combusted QMA filters to analyze ^{234}Th, POC and PON on the same filter, and the other aliquot

159 was filtered through QMA filters to analyze ^{210}Po and ^{210}Pb. Swimmers observed by naked eye

160 were picked from all samples. The activity of ^{234}Th in particles was measured by beta counting

161 as described for the water samples. POC and PON were determined with an EuroVector

162 Elemental Analyzer, pre-treating the filters with diluted HCl [*Knap et al.*, 1996]. The results

163 were corrected for POC and PON blanks (1.7 ± 0.1 and 0.35 ± 0.06 µmol, respectively),

164 representing on average 5 and 8% of the POC and PON measurements, respectively. The filters

165 for ^{210}Po and ^{210}Pb determination were spiked with ^{209}Po and stable Pb, digested using a mixture

166 of concentrated HNO_3, HCl and HF, evaporated to dryness and reconstructed with 1 M HCl.

167 Samples were processed and measured by alpha spectrometry as described for the water samples.

168 All data of particulate ^{234}Th, ^{210}Po, ^{210}Pb, and organic carbon and nitrogen concentrations are

169 available at http://doi.pangaea.de/10.1594/PANGAEA.858790.

170   2.4 Pigments

171   1-L seawater samples were taken from Niskin bottles attached to the CTD rosette from

172   three to four depths in the upper 30 m at eight stations. The samples were immediately filtered on

173   GF/F filters, frozen in liquid nitrogen, and stored at -80 °C until further analyses by high

174   performance liquid chromatography (HPLC) at the home laboratory. The samples were measured

175   using a Waters 600 controller equipped with an auto sampler (717 plus), a photodiode array

176   detector (2996), a fluorescence detector (2475) and the EMPOWER software. 50 µL of internal

177   standard (canthaxanthin) and 1.5 mL acetone were added to each filter vial and then

178   homogenized for 20 seconds in a Precellys® tissue homogenizer. After centrifugation the

179   supernatant liquids were filtered through 0.2 µm PTFE filters (Rotilabo) and placed in Eppendorf

180   cups. 100 µL-aliquots were transferred to the auto sampler (4 °C), premixed with 1 M

181   ammonium acetate solution in a 1:1 volume ratio just prior to analysis, and injected onto the

182   HPLC-system. Pigments were analyzed by reverse-phase HPLC using a VARIAN Microsorb-

183   MV3 C8 column (4.6x100 mm) and HPLC-grade solvents (Merck). Solvent A consisted of 70%

184   methanol and 30% 1 M ammonium acetate, and solvent B contained 100% methanol. The

185   gradient was modified after *Barlow et al.* [1997]. Eluting pigments were detected by absorbance

186   (440 nm) and fluorescence (Ex: 410 nm, Em: >600 nm). Pigments were identified by comparing

187   their retention times with those of pure standards. Additional confirmation for each pigment was

188   done by comparing spectra with on-line diode array absorbance spectra between 390 and 750 nm

189   stored in the library. Pigment concentrations were quantified based on peak areas of external

190   standards, which were spectrophotometrically calibrated using extinction coefficients published

191   by *Bidigare* [1991] and *Jeffrey et al.* [1997]. The taxonomic structure of the phytoplankton

192   groups (diatoms, dinoflagellates_1, dinoflagellates_2, haptophytes_3, haptophytes_4,

193   cryptophytes, prasinophytes_1, prasinophytes_2, pelagophytes and chlorophytes) was calculated

194   from marker pigment ratios using the CHEMTAX® program [*Mackey et al.*, 1996]. Pigment

195   ratios were constrained as suggested by *Higgins et al.* [2011] based on molecular analyses of 18S

196   rDNA [*Kilias et al.*, 2013] and microscopic examination of representative samples.

197   Phytoplankton size classes (micro-, nano-, and picoplankton) were estimated according to Uitz et

198   al. [2006] and Hirata et al. [2011], summarized by Taylor et al. [2011]. Microplankton

199   corresponded to phytoplankton with size between 20 and 200 µm, nanoplankton between 2 and

200   20 µm and picoplankton <2 µm. The phytoplankton classifications by group and size are

201   expressed as percentage of total chlorophyll *a* (Chl-a) biomass.

202   2.5 Primary production

203   In situ NPP was measured at eight stations using the ^{14}C uptake method [*Steemann*

204   *Nielsen*, 1952], with minor modifications as described in *Fernández-Méndez et al.* [2015].

205   Seawater, melted sea-ice cores and melt pond samples (one 200 mL sample per environment and

206   station) were spiked with 0.1 µCi mL^{-1} of ^{14}C labelled sodium bicarbonate (Moravek

207   Biochemicals, USA) and incubated for 12 hours at -1.3 °C under different scalar irradiances (0–

208   420 µmol photons m^{-2} s^{-1}). Depth-integrated in situ rates were calculated for each environment as

209   a function of the available photosynthetically active radiation (PAR) using the photosynthetic

210   parameters obtained in the photosynthesis vs. irradiance curves. Water column production was

211   integrated over the euphotic zone (1% of incoming irradiance) and sea-ice algae production over

212   the ice thickness.

213   At the same stations we calculated the integrated amount of NPP that potentially occurred

214   one and two weeks before sampling using the Central Arctic Ocean Primary Productivity

215   (CAOPP) model [*Fernández-Méndez et al.*, 2015]. This model calculates NPP from incident

216   light and sea-ice conditions based on different remote-sensing datasets on the basis of

217   photosynthesis-irradiance curves measured during the cruise. NPP was calculated for each day

218   during the 14 days prior to sampling, summed up to integrate values for the one- and two-week

219   period before sampling, and divided by 7 and 14 days, respectively, to obtain average daily rates

220   for these two periods.

221   Annual new NPP was calculated from the nitrate drawdown in the mixed layer since

222   previous winter at nine stations, as described in *Fernández-Méndez et al.* [2015]. The annual

223   total inorganic nitrogen uptake was then transformed to carbon units using the Redfield ratio

224   106C:16N [*Smith et al.*, 1997; *Codispoti et al.*, 2013], giving annual new NPP estimates for sea

225   ice and water column during the Arctic productive season. To calculate an average daily rate we

226   assumed a productive season of 120 days [*Gradinger et al.*, 1999]. Although most of the new

227   NPP occur before late summer, we note that these estimates may be underestimated mainly for

228   the first stations sampled in August. This method assumes that lateral input of nitrate from rivers

229   or shelves is negligible, which should be the case of the present study (>81ºN) due to its

230 consumption in Arctic shelf waters [*Le Fouest et al.*, 2013]. Further, this method do not take into

231 consideration nitrification and upward flux of nitrate, which are assumed to have a relatively

232 small contribution to the nitrate concentrations in the mixed layer in comparison with the

233 biological uptake.

234 **3 Results**

235 3.1 Study area

236 Sea-ice conditions, phytoplankton communities and primary production rates in the study

237 area are described below and summarized in Table 1.

238 **Table 1:** Location and date of the stations sampled during the ARK-XXVII/3 cruise together with information on
239 oceanographic and sea-ice conditions, Chl-a inventory at 30 m depth, phytoplankton classifications by size and
240 group, and NPP estimates (see text for further details). The methods used to estimate POC export fluxes in each
241 station are specified as: Th/U (^{234}Th/^{238}U), Po/Pb (^{210}Po/^{210}Pb) and ST (sediment traps, [Lalande et al., 2014]).

| Station	1	2	3	4	5	6	7	8	9
Polarstern station #	PS80/ 224	PS80/ 237	PS80/ 255	PS80/ 277	PS80/ 323	PS80/ 335	PS80/ 349	PS80/ 360	PS80/ 384
Longitude (ºE)	31.19	75.99	110.11	129.83	131.12	123.47	60.97	57.07	17.59
Latitude (ºN)	84.03	83.92	83.08	82.89	81.93	85.17	87.93	88.80	84.37
Date (2012)	9-11 Aug.	14-16 Aug.	20-22 Aug.	25-26 Aug.	4-5 Sept.	7-9 Sept.	18-19 Sept.	22-23 Sept.	28-29 Sept.
Methods	Th/U, Po/Pb, ST	Th/U, Po/Pb, ST	Th/U, Po/Pb, ST	Th/U, Po/Pb, ST	Th/U, ST	Th/U, Po/Pb, ST	Th/U, Po/Pb, ST	Th/U, Po/Pb, ST	Th/U, ST
Euphotic zone depth (m)[a]	24	29	30	29	33	29	15	7	
Mixed layer depth (m)	16	20	18	22	20	25	29	30	22
Sea-ice thickness (m)[a,b]	1.0	1.3	0.9	0.9	0.8	0.7	1.6	1.8	1.2
Sea ice-concentration (%)[a,b]	80	80	70	80	60	50	100	100	100
Chl-a inventory (mg m^{-2})	4.8	22.8	8.9	7.0	8.9	11.2	6.1	3.3	2.5
Phytoplankton size (% Chl-a biomass)									
Microplankton	36	29	38	54	36	14	34	nd	39
Nanoplankton	22	0	2	13	4	28	44	nd	32
Picoplankton	42	71	60	33	60	58	22	nd	29
Phytoplankton group (% Chl-a biomass)									
Diatoms	19	5	4	44	27	3	23	nd	22
Dinoflagellates_1	0	0	8	2	0	0	0	nd	0
Dinoflagellates_2	8	0	9	0	2	11	1	nd	12
Haptophytes_3	21	0	0	4	0	26	61	nd	19
Haptophytes_4	0	0	8	5	3	3	2	nd	4

Cryptophytes	0	0	1	18	10	0	0	nd	0
Prasinophytes_1	51	33	8	26	27	35	12	nd	22
Prasinophytes_2	0	61	61	0	28	0	0	nd	0
Pelagophytes	0	0	1	1	3	0	0	nd	21
Chlorophytes	0	0	0	0	0	21	1	nd	0
NPP estimates (mmol C m^{-2} d^{-1})									
In-situ	3.3	2.7	1.3	0.5	5.0	2.3	0.2	0.1	nd
One week	2.3	2.3	2.2	3.5	1.8	1.9	0.6	0.5	nd
Two weeks	2.4	2.5	2.2	3.3	2.2	2.3	0.8	0.6	nd
Annual	3.3	4.8	2.1	2.9	5.6	3.2	11.9	9.9	7.9

242 nd = no available data. [a] Data from *Fernández-Méndez et al.* [2015]. [b] Data from *Katlein et al.* [2014].

243 ### 3.1.1 Oceanographic and sea-ice conditions

244 Stations were located over the deep Arctic (>3000 m) in the Nansen (stations 1-3 and 9)
245 and Amundsen Basins (stations 4-8, Figure 1). The sea-ice conditions encountered during the
246 expedition are described in *Katlein et al.* [2014]. Stations located north of 87ºN (stations 7 and 8)
247 had multi-year ice, 1.6-1.8 m thick, while the rest consisted of degraded first-year ice of 0.7-1.3
248 m. The sea-ice concentration varied from 50 to 80% at stations 1-6, but it was 100% at those
249 stations visited in mid-late September (stations 7-9, Table 1). The coverage of melt-ponds ranged
250 from 10 to 50% [*Boetius et al.*, 2013]. The euphotic zone (1% of incoming irradiance) was on
251 average 25 m deep and was nutrient depleted by phytoplankton consumption: i) silicate-depleted
252 at stations 1-3; ii) nitrate-depleted at stations 4 and 5; and iii) silicate, nitrate and phosphate-
253 depleted at stations 6-9 [*Fernández-Méndez et al.*, 2015]. The mixed layer was on average 22 m
254 thick and was defined by the depth where density increased from its surface value to 20% of the
255 difference between 100 m and the surface [*Shaw et al.*, 2009] using the CTD profiles obtained
256 during the cruise (doi:10.1594/PANGAEA.802904). The winter mixed layer depth was found at
257 around 55 m [*Fernández-Méndez et al.*, 2015] above the lower halocline (salinity range: 33.5-
258 34.5) [*Rudels*, 2009], which reached depths down to 150 m. The potential temperature maximum
259 indicative of the Atlantic Water core was found between the depth range 180-290 m. Underneath
260 the Atlantic layer, Arctic intermediate waters as well as deep and bottom waters were located.

261
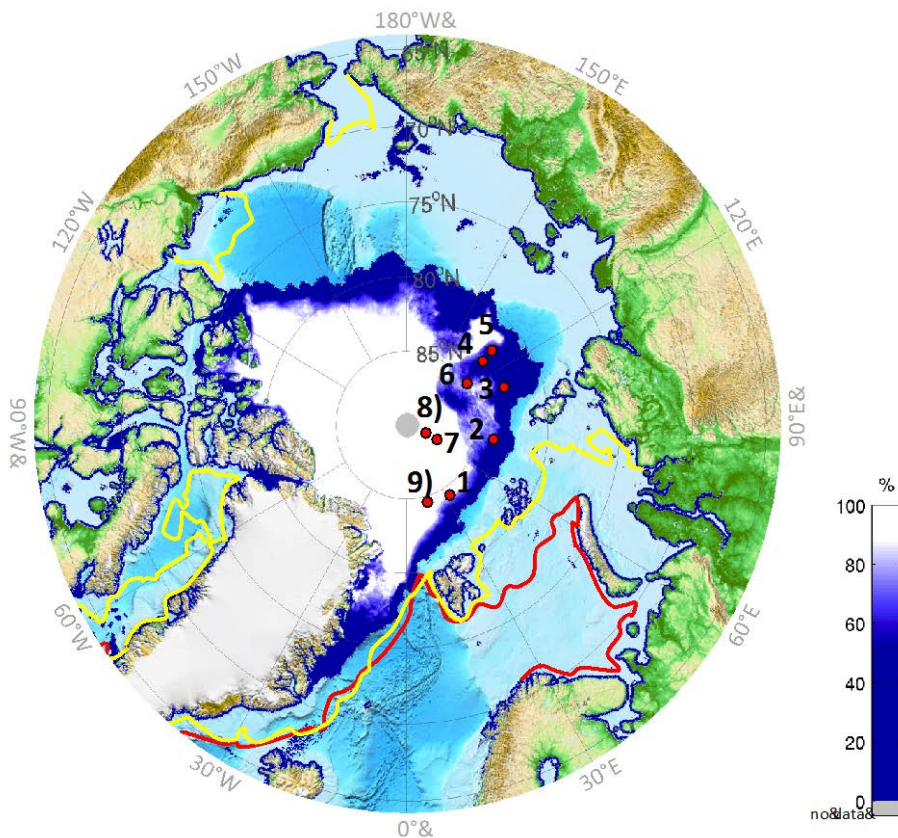
Figure 1: Location of sea-ice stations sampled during the IceArc cruise (ARK-XXVII/3, August-September 2012) (red dots). Average sea-ice concentration in September 2012. Contour lines represent the sea-ice extent in February (red) and July (yellow) 2012. Sea-ice concentration data were obtained from http://www.meereisportal.de (grant: REKLIM-2013-04) [*Spreen et al.*, 2008].

3.1.2 Biology

The Chl-a inventories in the upper 30 m of the water column were on average 8.4 ± 6.1 mg m^{-2}, with a maximum at station 2 (22.8 mg m^{-2}) and a minimum at station 9 (2.5 mg m^{-2}). The phytoplankton community was picoplankton dominated at many stations (1, 2, 3, 5 and 6), accounting for ~40-70% of the total Chl-a biomass. At those stations prasinophytes were the most relevant group with a relative biomass up to 95%. Large cells dominated the community at station 4 with a significant contribution from diatoms (44%), while nanoplankton prevailed at station 7 with a dominance of haptophytes (63%). Finally, station 9 had a similar biomass distribution between size classes (Table 1).

The integrated in situ NPP rates in the euphotic zone, sea ice and melt ponds ranged from 0.1 mmol C m^{-2} d^{-1} at the northernmost station (8), to 5.0 mmol C m^{-2} d^{-1} at the southernmost station (5). In situ NPP was highest at the picoplankton-dominated stations (>1.3 mmol C m^{-2} d^{-}

278   [1]). The daily NPP estimates during one and two weeks prior to sampling were higher than the in

279   situ estimates by a factor of 2-7 at stations 3, 4, 7, 8, while they were a factor of 3 lower at

280   station 5. These estimates were comparable at stations 1, 2 and 6. The annual new primary

281   production estimates compared well with the in situ, one- and two-week daily estimates from

282   stations 1 to 6. However, north of 87ºN (stations 7 and 8) the annual estimates were higher than

283   the average of the other estimates by a factor >20 (~10-12 mmol C m^{-2} d^{-1}, Table 1).

284   3.2 Total ^{234}Th/^{238}U and ^{210}Po/^{210}Pb

285   3.2.1 Seawater profiles

286   The profiles of the total activities of ^{234}Th and ^{238}U, and ^{210}Po and ^{210}Pb are illustrated in

287   Figure 2.

^{234}Th and ^{238}U
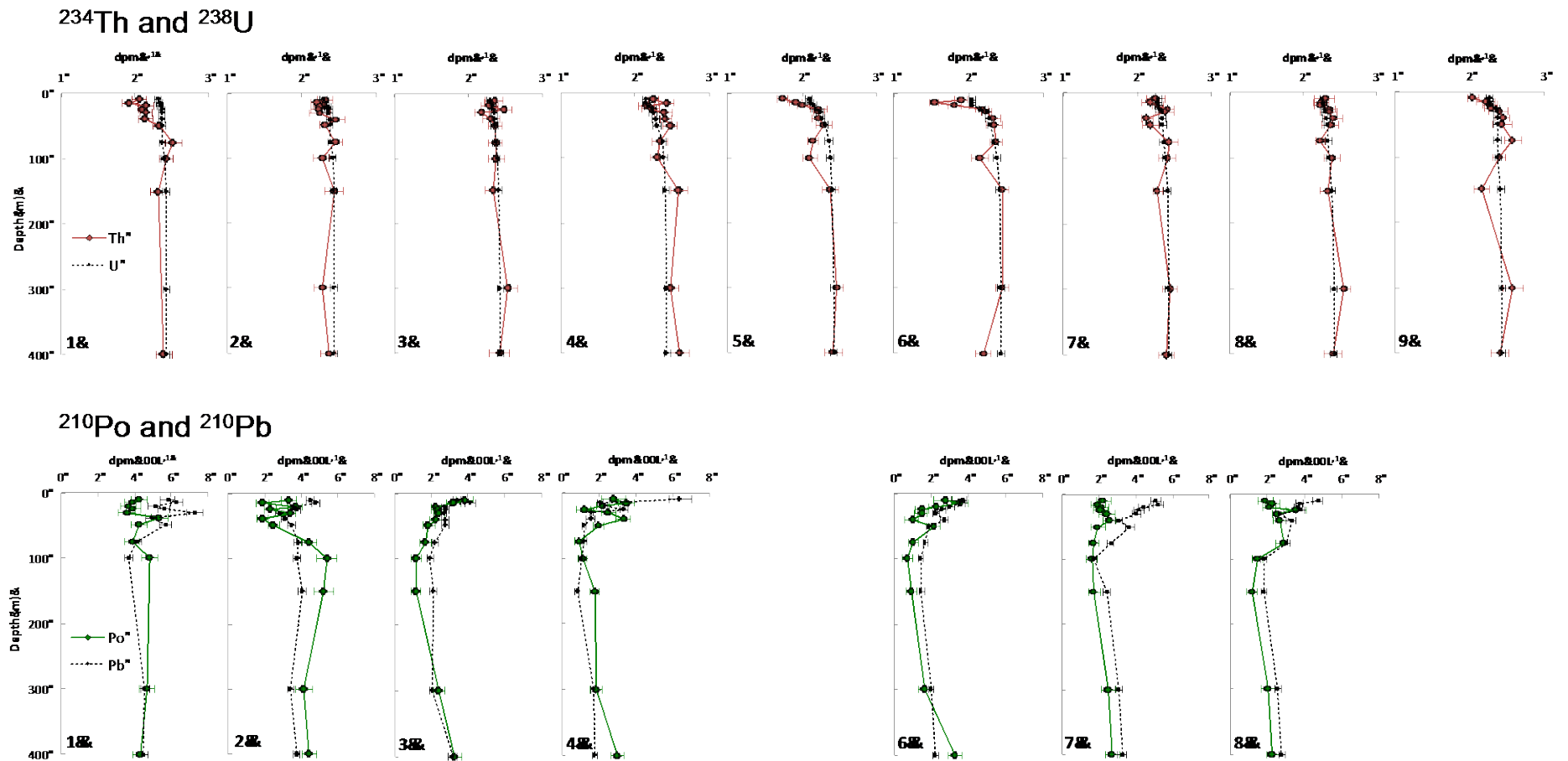
^{210}Po and ^{210}Pb

288   **Figure 2:** Vertical activity profiles for ^{234}Th (red solid line) and ^{238}U (dotted line) (top panels) and for ^{210}Po (green solid line) and ^{210}Pb (dotted line) (bottom
289   panels), from 10 to 400 m depth. ^{238}U was derived from salinity [*Owens et al.*, 2011].

290   The specific activities of each radionuclide ranged from 1.54 ± 0.06 to 2.59 ± 0.13 dpm

291   L^{-1} for ^{234}Th, 2.04 ± 0.05 to 2.44 ± 0.05 dpm L^{-1} for ^{238}U, 0.7 ± 0.3 to 5.4 ± 0.5 dpm 100L^{-1} for

292   ^{210}Po, and 0.84 ± 0.09 to 7.3 ± 0.4 dpm 100L^{-1} for ^{210}Pb. Within the upper 25 m of the water

293   column, significant deficits of ^{234}Th (i.e. ^{234}Th/^{238}U <0.9, given uncertainties) were observed at

294   stations 1, 5 and 6, while significant deficits of ^{210}Po (i.e. ^{210}Po/^{210}Pb <0.8, given uncertainties)

295   were detected at all the stations. Below 25 m depth, deficits of ^{234}Th were detected at one single

296   depth at stations 5 and 9 (100-150 m), but deficits of ^{210}Po were found at every station usually at

297   several depths (30-150 m). Excesses of ^{234}Th (i.e. ^{234}Th/^{238}U >1.1) were not observed at any

298   profile below 25 m, whereas excesses of ^{210}Po (i.e. ^{210}Po/^{210}Pb >1.2) were observed at four

299   stations (1, 2, 4 and 6).

300   Station 1 showed deficits of ^{234}Th and ^{210}Po within the upper 50 m: 11500 ± 2100 and

301   770 ± 120 dpm m^{-2}, respectively. Station 6 also showed deficits of both isotopes, down to 25 m

302   for ^{234}Th (160 ± 40 dpm m^{-2}) and 150 m for ^{210}Po (930 ± 200 dpm m^{-2}). At five stations (2, 3, 4,

303   7 and 8) ^{234}Th was not significantly depleted in the upper water column. On the contrary, at those

304   stations the integrated ^{210}Po deficits in the upper water column (50-150 m) ranged from 130 ±

305   150 to 1640 ± 220 dpm m^{-2}. The integrated excesses of ^{210}Po observed at stations 2 (30, 100-300

306   m) and 4 (15, 30-50, 150, 400 m) exceeded the integrated deficits observed in the surface water.

307   Finally, at stations 5 and 9 (only ^{234}Th sampling), ^{234}Th was in equilibrium with ^{238}U throughout

308   the upper 400 m with only a few exceptions.

309   3.2.2 ^{234}Th and ^{210}Po fluxes

310   The ^{234}Th and ^{210}Po fluxes (F_D) are attributed to scavenging of ^{234}Th and ^{210}Po onto

311   sinking particles. The fluxes were calculated using a steady state (SS) model, neglecting

312   advective and diffusive fluxes [*Buesseler et al.*, 1992]:

$$F_D = \lambda_D(A_P - A_D)$$

313   where D stands for "daughter" (^{234}Th or ^{210}Po) and P for "parent" (^{238}U or ^{210}Pb, respectively).

314   λ_D is the decay constant of ^{234}Th (0.029 d^{-1}) or ^{210}Po (0.0050 d^{-1}), and ($A_P - A_D$) is the integrated

315   daughter deficit with respect to its parent (dpm m^{-2}). The fluxes calculated down to 25, 50, 100

316   and 150 m are listed in Table 2.

317

318 **Table 2:** [234]Th and [210]Po export fluxes assuming steady state conditions at 25, 50, 100 and 150 m.

Station	Depth (m)	[234]Th fluxes (dpm m^{-2} d^{-1})			[210]Po fluxes (dpm m^{-2} d^{-1})		
1	25	200	±	50	2.1	±	0.4
	50	330	±	60	3.9	±	0.6
	100	230	±	130	4.3	±	1.0
	150	280	±	190	1.8	±	1.5
2	25	40	±	50	1.6	±	0.3
	50	70	±	70	2.4	±	0.4
	100	100	±	120	1.3	±	0.9
	150	200	±	200	-2.2	±	1.5
3	25	-20	±	50	0.2	±	0.3
	50	10	±	70	0.8	±	0.4
	100	20	±	120	2.5	±	0.7
	150	70	±	200	4.5	±	1.0
4	25	-70	±	40	2.2	±	0.6
	50	-160	±	60	1.0	±	0.7
	100	-160	±	120	0.8	±	0.8
	150	-220	±	180	-0.4	±	1.0
5	25	170	±	40	nd		
	50	190	±	60	nd		
	100	440	±	110	nd		
	150	660	±	180	nd		
6	25	160	±	40	0.9	±	0.3
	50	130	±	60	2.1	±	0.4
	100	180	±	120	3.2	±	0.7
	150	310	±	190	4.7	±	1.0
7	25	20	±	50	3.4	±	0.4
	50	90	±	70	5.0	±	0.5
	100	90	±	140	7.2	±	0.8
	150	160	±	200	8.2	±	1.1
8	25	0	±	60	2.5	±	0.4
	50	-50	±	80	3.0	±	0.5
	100	0	±	120	3.7	±	0.9
	150	20	±	190	4.9	±	1.1
9	25	90	±	40	nd		
	50	60	±	70	nd		
	100	-110	±	140	nd		
	150	70	±	190	nd		

319 nd = no available data

320   The [234]Th fluxes were negligible or very low at 5 out of 9 stations (2, 3, 4, 7 and 8). At

321 stations 1, 5 and 6, the [234]Th fluxes averaged 175 ± 19 dpm m^{-2} d^{-1} at 25 m, 210 ± 100 dpm m^{-2} d^{-}

322   [1] at 50 m, 280 ± 140 dpm m^{-2} d^{-1} at 100 m and 400 ± 200 dpm m^{-2} d^{-1} at 150 m. At station 9 the

323   already low ^{234}Th flux at 25 m (90 ± 40 dpm m^{-2} d^{-1}) became negligible in deeper waters. The

324   ^{210}Po fluxes were significant at all the stations, averaging 1.8 ± 1.1 dpm m^{-2} d^{-1} at 25 m, 2.6 ± 1.5

325   dpm m^{-2} d^{-1} at 50 m, 3 ± 2 dpm m^{-2} d^{-1} at 100 m and 3 ± 3 dpm m^{-2} d^{-1} at 150 m. The ^{210}Po fluxes

326   did not decrease with depth at the majority of stations (1, 3, 6, 7 and 8), whereas at stations 2 and

327   4 the fluxes became negligible at 100-150 m.

328   3.3. Particulate fraction

329   Particulate ^{234}Th, ^{210}Po, ^{210}Pb, and organic carbon and nitrogen concentrations in large

330   particles are given in Table 3, as well as the ^{210}Po/^{210}Pb and molar C/N ratios.

331   The mean ^{234}Th activities in particles decreased with depth, ranging from ~1 dpm 100L^{-1}

332   at 25 m to ~0.3 dpm 100L^{-1} at 150 m. ^{210}Po activities were on average ~0.04 dpm 100L^{-1} at 25 m

333   and ~0.02 dpm 100L^{-1} below that depth, while ^{210}Pb activities were ~0.06 dpm 100L^{-1} at 25 and

334   50 m, and ~0.02 dpm 100L^{-1} at 100 and 150 m. The variation between stations was large, with

335   deviations from those means of >50% for ^{234}Th, >80% for ^{210}Po and >100% for ^{210}Pb. Only

336   about 0.3% of the total activity of ^{234}Th in water, 1.1% of ^{210}Po and 1.7% of ^{210}Pb was associated

337   with large particles. The maximum particulate activities were found at stations 2 and 3 and the

338   minimum at stations 7 and 8 (negligible in some instances for ^{210}Po and ^{210}Pb). The ^{210}Po/^{210}Pb

339   ratios ranged from 0.2 to 6 (average: 1.2 ± 1.4, n = 18), varying considerably between stations

340   and depths.

341   The POC and PON concentrations were highest at 25 m, averaging 0.23 ± 0.08 and 0.028

342   ± 0.011 µmol L^{-1} (n = 8), respectively. Below that depth the concentrations decreased by a factor

343   of 3. The mean C/N ratio was similar at all the investigated depths, averaging 8.8 ± 1.9 (n = 34).

344   Table 4 displays the POC/^{234}Th and POC/^{210}Po ratios (C/Th and C/Po) at 25, 50, 100 and

345   150 m. The average ratios at the different horizon depths ranged from 17 to 40 µmol dpm^{-1} for

346   C/Th and from 300 to 1100 µmol dpm^{-1} for C/Po. The ratios did not change significantly with

347   depth (Kruskal-Wallis test, p >0.05).

348 **Table 3:** Particulate ^{234}Th, ^{210}Po, ^{210}Pb, and organic carbon and nitrogen concentrations, and ^{210}Po/^{210}Pb and molar C/N ratios in particles >53 μm.

Station	Depth (m)	Part. ^{234}Th (dpm 100L^{-1})	Part. ^{210}Po (dpm 100L^{-1})	Part. ^{210}Pb (dpm 100L^{-1})	^{210}Po/^{210}Pb	POC (μmol C L^{-1})	PON (μmol N L^{-1})	C/N (mol:mol)
1	15	0.45 ± 0.03	0.026 ± 0.003	0.0042 ± 0.0012	6 ± 2	0.25	0.038	6.6
	50	nd	nd	nd	nd	nd	nd	nd
	90	0.335 ± 0.019	0.008 ± 0.003	0.0144 ± 0.0018	0.6 ± 0.2	0.074	0.0092	8.1
	190	0.138 ± 0.008	0.011 ± 0.002	0.0057 ± 0.0011	1.8 ± 0.5	0.034	0.0054	6.3
2	25	nd	nd	nd	nd	nd	nd	nd
	50	1.71 ± 0.12	0.032 ± 0.006	0.031 ± 0.003	1.0 ± 0.2	0.23	0.034	6.7
	100	1.86 ± 0.12	0.120 ± 0.011	0.073 ± 0.004	1.6 ± 0.2	0.12	0.020	6.3
	150	0.89 ± 0.06	0.050 ± 0.007	0.055 ± 0.004	0.91 ± 0.14	0.042	0.0068	6.1
3	25	1.63 ± 0.09	0.066 ± 0.010	0.217 ± 0.010	0.30 ± 0.05	0.27	0.033	8.1
	50	1.60 ± 0.11	0.054 ± 0.014	0.221 ± 0.011	0.24 ± 0.07	0.15	0.020	7.8
	100	0.215 ± 0.012	<0.003	0.039 ± 0.003	-	0.032	0.0043	7.4
	150	0.51 ± 0.02	0.035 ± 0.006	0.040 ± 0.004	0.9 ± 0.2	0.087	0.010	8.5
4	25	0.55 ± 0.03	0.025 ± 0.003	0.044 ± 0.003	0.57 ± 0.08	0.28	0.029	9.8
	50	0.47 ± 0.03	0.015 ± 0.003	0.031 ± 0.002	0.47 ± 0.12	0.036	0.0056	6.4
	100	0.276 ± 0.010	<0.003	0.0152 ± 0.0016	-	0.097	0.014	7.0
	150	0.43 ± 0.02	0.007 ± 0.003	0.023 ± 0.002	0.31 ± 0.15	0.058	0.0078	7.5
5	25	1.50 ± 0.10	nd	nd	nd	0.38	0.047	8.0
	50	0.88 ± 0.06	nd	nd	nd	0.14	0.016	8.5
	100	0.414 ± 0.016	nd	nd	nd	0.097	0.011	9.2
	150	0.58 ± 0.03	nd	nd	nd	0.061	0.0075	8.2
6	25	1.25 ± 0.08	0.077 ± 0.006	0.106 ± 0.005	0.73 ± 0.06	0.15	0.014	11.1
	50	0.250 ± 0.014	0.006 ± 0.003	0.026 ± 0.002	0.21 ± 0.12	0.025	0.0025	10.1
	100	0.094 ± 0.005	<0.003	0.008 ± 0.002	-	0.015	0.0014	10.1
	150	0.096 ± 0.009	0.013 ± 0.003	0.0059 ± 0.0016	2.2 ± 0.8	0.012	0.00090	13.6
7	25	0.42 ± 0.02	0.0126 ± 0.0018	0.0076 ± 0.0014	1.7 ± 0.4	0.23	0.023	10.0
	50	0.062 ± 0.007	<0.003	<0.003	-	0.029	0.0028	10.6
	100	0.061 ± 0.009	<0.003	0.0040 ± 0.0018	-	0.088	0.0074	11.9
	150	0.078 ± 0.006	0.009 ± 0.003	<0.003	-	0.036	0.0029	12.4
8	25	0.51 ± 0.02	0.009 ± 0.003	0.010 ± 0.002	0.9 ± 0.3	0.16	0.020	8.1
	50	0.286 ± 0.016	0.008 ± 0.003	0.026 ± 0.003	0.31 ± 0.13	0.049	0.0051	9.6
	100	0.133 ± 0.014	<0.003	0.012 ± 0.003	-	0.080	0.0070	11.5
	150	0.100 ± 0.008	<0.003	0.0040 ± 0.0018	-	0.032	0.0040	8.2
9	25	1.34 ± 0.10	nd	nd	nd	0.15	0.020	7.4
	50	0.64 ± 0.03	nd	nd	nd	0.088	0.0091	9.7
	100	0.229 ± 0.011	nd	nd	nd	0.069	0.0077	9.0
	150	0.18 ± 0.02	nd	nd	nd	0.059	0.0064	9.3

349   nd = no available data

350   3.4 POC fluxes

351   The POC fluxes were calculated multiplying the ^{234}Th and ^{210}Po fluxes derived

352   from the SS model by the C/Th and C/Po ratios in large particles, respectively (Table 4).

353   **Table 4:** Particulate POC/^{234}Th and POC/^{210}Po ratios (C/Th and C/Po), and POC fluxes derived from
354   ^{234}Th and ^{210}Po.

Station	Depth (m)	C/Th (µmol C dpm^{-1})			C/Po (µmol C dpm^{-1})			POC fluxes (mmol C m^{-2} d^{-1})					
								^{234}Th-derived			^{210}Po-derived		
1	15	56	±	4	970	±	100	7	±	2	1.2	±	0.4
	50	nd			nd			nd			nd		
	90	22.1	±	1.3	900	±	400	5	±	3	4	±	2
	190	25.0	±	1.5	330	±	70	10	±	6	0.1	±	0.7
2	25	nd			nd			nd			nd		
	50	13.2	±	0.9	700	±	120	0.9	±	0.9	1.7	±	0.4
	100	6.7	±	0.5	104	±	9	0.7	±	0.8	0.13	±	0.09
	150	4.7	±	0.3	83	±	12	0.9	±	0.9	-0.19	±	0.13
3	25	16.3	±	0.9	400	±	60	-0.4	±	0.8	0.06	±	0.14
	50	9.6	±	0.6	280	±	80	0.1	±	0.7	0.23	±	0.14
	100	14.8	±	0.8	-			0	±	2	-		
	150	16.9	±	0.8	250	±	40	1	±	3	1.1	±	0.3
4	25	51	±	3	1140	±	140	-4	±	2	2.5	±	0.7
	50	7.7	±	0.4	250	±	60	-1.2	±	0.5	0.3	±	0.2
	100	35.2	±	1.3	-			-6	±	4	-		
	150	13.6	±	0.6	800	±	400	-3	±	2	-0.3	±	0.9
5	25	25.1	±	1.7	nd			4.3	±	1.0	nd		
	50	15.6	±	1.0	nd			2.9	±	0.9	nd		
	100	23.5	±	0.9	nd			10	±	3	nd		
	150	10.5	±	0.5	nd			7	±	2	nd		
6	25	12.2	±	0.8	197	±	14	1.9	±	0.5	0.18	±	0.07
	50	10.1	±	0.5	500	±	200	1.3	±	0.6	1.0	±	0.5
	100	15.5	±	0.8	-			3	±	2	-		
	150	12.7	±	1.2	90	±	20	4	±	2	0.44	±	0.13
7	25	54	±	3	1800	±	300	1	±	3	6.3	±	1.1
	50	48	±	6	-			4	±	3	-		
	100	150	±	20	-			10	±	20	-		
	150	47	±	4	390	±	110	7	±	9	3.2	±	1.0
8	25	32.3	±	1.4	1900	±	600	0	±	2	4.8	±	1.6
	50	17.1	±	1.0	600	±	300	-0.9	±	1.3	1.8	±	1.3
	100	60	±	6	-			0	±	7	-		
	150	32	±	3	-			1	±	6	-		
9	25	11.2	±	0.8	nd			1.0	±	0.5	nd		
	50	13.7	±	0.8	nd			0.9	±	0.9	nd		
	100	30.2	±	1.4	nd			-3	±	4	nd		
	150	32	±	4	nd			2	±	6	nd		

355   nd = no available data.

356   The ^{234}Th-derived POC fluxes ranged from negligible to 10 mmol C m^{-2} d^{-1} and

357   averaged 1.3 to 4 mmol C m^{-2} d^{-1} at 25, 50, 100 and 150 m. The ^{210}Po-derived POC

358   fluxes ranged from negligible to 6.3 mmol C m^{-2} d^{-1} and were on average from 0.8 to 3

359   mmol C m^{-2} d^{-1} at the same depths. The POC fluxes estimated using the two proxies

360 were not significantly different considering all depths together, or each depth

361 individually (Wilcoxon test, p >0.05).

362 **4 Discussion**

363 In this study we have used two pairs of radionuclides, ^{234}Th/^{238}U and

364 ^{210}Po/^{210}Pb, as tools to estimate POC fluxes in the Eurasian Basin of the Arctic Ocean in

365 summer 2012. Deficits of ^{234}Th and ^{210}Po are attributed to particle export, while the

366 excesses of these radionuclides evidence their release from sinking particles by means

367 of remineralization or particle disaggregation into the suspended pool. Their

368 simultaneous application allows integrating a temporal scale over a span of weeks

369 (^{234}Th mean life = 35 days) to months (^{210}Po mean life = 200 days).

370 4.1 ^{234}Th/^{238}U

371 4.1.1 ^{234}Th export fluxes

372 ^{234}Th export fluxes were calculated using a SS model because the stations were

373 not reoccupied during the expedition. Yet in a review study *Savoye et al.* [2006] did not

374 find significant differences between the SS and non-steady state (NSS) models at low

375 flux rates (<800 dpm m^{-2} d^{-1}), which is the case of the present work.

376 Significant ^{234}Th fluxes within the upper 150 m of the water column were

377 obtained at stations 1, 5 and 6, and at stations 7 and 9 only at one single depth (Table 2).

378 The ^{234}Th fluxes ranged from negligible to 660 dpm m^{-2} d^{-1}, averaging 120 ± 140 dpm

379 m^{-2} d^{-1} (n = 36). Our results are one order of magnitude lower than the ^{234}Th flux

380 average reported by *Le Moigne et al.* [2013b] for the world ocean (1200 ± 900 dpm m^{-2}

381 d^{-1}; 75-210 m; n = 421). Previous research conducted in the central Arctic, mainly

382 during summer, has also revealed low export fluxes escaping from the ocean surface

383 (Figure 3). *Cai et al.* [2010] reported an average of 90 ± 300 dpm m^{-2} d^{-1} (n = 26) in the

384 most extensive study of ^{234}Th over the central basins to date, and *Moran et al.* [1997]

385 and *Gustafsson and Andersson* [2012] reported similar flux averages of 190 ± 140 dpm

386 m^{-2} d^{-1} (n = 7) and 130 ± 100 dpm m^{-2} d^{-1} (n = 3), respectively. *Le Moigne et al.* [2015]

387 reported ^{234}Th fluxes of 140 ± 210 dpm m^{-2} d^{-1} in the ice covered Fram Strait, which is

388 also in line with our results. Nevertheless, other studies have reported high ^{234}Th export

389 fluxes (>2000 dpm m^{-2} d^{-1}) at specific locations in the Canada Basin [*Ma et al.*, 2005],

390 although they are more typical of the shelf environment [e.g. *Coppola et al.*, 2002;

391 *Lepore et al.*, 2007] (Figure 3). Overall, the ^{234}Th flux data presented here and the

392 limited data available to date illustrate the central Arctic basins as deserts in terms of

393 particle export during summer.

394
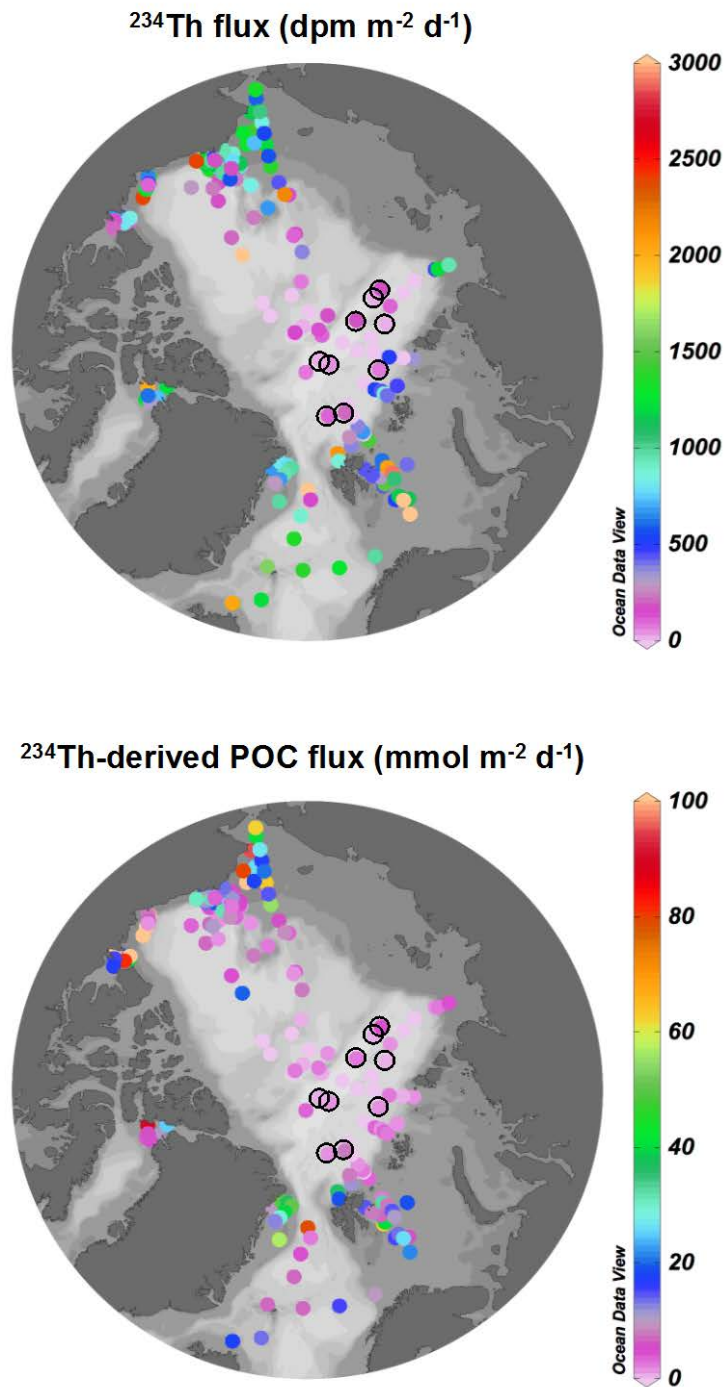
Figure 3: Compilation of [234]Th flux data (upper panel) and [234]Th-derived POC flux data (lower panel) from the Arctic Ocean (236 stations) [*Cochran et al.*, 1995b; *Moran et al.*, 1997, 2005; *Moran and Smith*, 2000; *Amiel et al.*, 2002; *Coppola et al.*, 2002; *Baskaran et al.*, 2003; *Chen et al.*, 2003; *Ma et al.*, 2005; *Trimble and Baskaran*, 2005; *Lepore et al.*, 2007; *Lalande et al.*, 2007, 2008; *Amiel and Cochran*, 2008; *Yu et al.*, 2010, 2012; *Cai et al.*, 2010; *Gustafsson and Andersson*, 2012; *Le Moigne et al.*, 2015; this study]. Black circles indicate the results obtained in this study. The depth horizon taken to calculate the POC export fluxes ranges from 25 to 200 m.

402   4.1.2 ^{234}Th-derived POC export fluxes

403   The mean ^{234}Th-derived POC export fluxes measured in the upper 150 m were 3 ± 3

404   mmol C m^{-2} d^{-1} (n = 34), with a maximum of 10 mmol C m^{-2} d^{-1} (Table 4). At the bottom of the

405   euphotic zone (~25 m) the fluxes ranged from negligible to 7 mmol C m^{-2} d^{-1} (average: 2 ± 2

406   mmol C m^{-2} d^{-1}, n = 8). These results are in very good agreement with the POC fluxes measured

407   with cylindrical sediment traps (HydroBios, Kiel, Germany) deployed under the ice during

408   periods of 24-53 hours from station 1 to 9 [*Lalande et al.*, 2014]. The sediment trap results

409   ranged from 0.4 to 9 mmol C m^{-2} d^{-1} (average: 3 ± 3 mmol C m^{-2} d^{-1}, n = 9). The in situ NPP

410   rates showed positive correlations with ^{234}Th fluxes at 25 m (p <0.05; Spearman correlation

411   coefficient, ρ = 0.83; n = 8), ^{234}Th-derived POC fluxes at 25 m (p <0.05; ρ = 0.78; n = 7) and

412   sediment trap-derived POC fluxes at 25 m (p <0.05; ρ = 0.83; n = 8), which indicates enhanced

413   particle fluxes with increasing NPP. Our results also compare well with previous literature values

414   from sediment traps deployed at 150-175 m north of the Laptev Sea continental margin in

415   August-September during the years 95/96 and 05/06 (~0.5-2.5 mmol C m^{-2} d^{-1}) [*Fahl and*

416   *Nöthig*, 2007; *Lalande et al.*, 2009] and ^{234}Th-derived POC fluxes in the central Arctic (Figure

417   3). *Cai et al.* [2010] documented very low POC export fluxes (average: 0.2 ± 1.0 mmol C m^{-2} d^{-1},

418   n = 26) across the deep Arctic, suggesting that they were a consequence of low biological

419   productivity. Our low POC export flux estimates are in good agreement with the low NPP

420   observed in the present study within the ^{234}Th time window (in situ, one- and two-week

421   estimates; ≤5 mmol C m^{-2} d^{-1}; Table 1).

422   4.1.3 Relationships with phytoplankton community

423   We did not find any significant relationship between the ^{234}Th data (particulate ^{234}Th

424   activity, ^{234}Th fluxes and ^{234}Th-derived POC fluxes) and the phytoplankton size structure at the

425   sampling time, although two correlations were obtained with regards to the phytoplankton

426   composition. The relative biomass of prasinophytes_1 was positively correlated with ^{234}Th fluxes

427   (p <0.05; ρ = 0.75; n = 8) and ^{234}Th-derived POC fluxes (p <0.05; ρ = 0.77; n = 7) at 25 m. This

428   suggests that prasinophytes_1 would have contributed significantly to vertical export fluxes

429   during the late summer in 2012 when picoplankton, and particularly prasinophytes, were the

430   predominant group in terms of biomass (Prasinophytes_1 and 2, Table 1). Prasinophytes are

431   green algae that can be usually found in the eukaryotic picoplankon fraction. A molecular study

432 by *Metfies et al.* [2016] corroborates the biomass dominance of picoplankton in the upper water

433 column during our expedition and identifies the prasinophyte *Micromonas* spp. as its major

434 constituent. Our finding is in line with recent observations that reveal that small cells are

435 important contributors to POC export fluxes in diverse oceanic regimes [e.g. *Richardson and*

436 *Jackson*, 2007; *Lomas and Moran*, 2011; *Durkin et al.*, 2015; *Mackinson et al.*, 2015; *Puigcorbé*

437 *et al.*, 2015]. Prasinophytes, including *Micromonas* spp., are common in the central Arctic

438 [*Booth and Horner*, 1997; *Sherr et al.*, 2003; *Zhang et al.*, 2015], and are considered to be

439 among the most abundant photosynthetic cells in pan-Arctic waters [*Lovejoy et al.*, 2007].

440 Genetic analyses in trap samples revealed that prasinophytes contributed to downward fluxes in

441 the Sargasso Sea [*Amacher et al.*, 2013], but to our knowledge, this has not been observed before

442 in Arctic waters. It is relevant to note that neither molecular nor pigment techniques inform about

443 whether they sink as single cells or as part of other export pathways.

444 The pathways by which picoplankton cells can be removed from the ocean surface are

445 fundamentally: i) zooplankton grazing and subsequent incorporation into fecal pellets [*Waite et*

446 *al.*, 2000; *Wilson and Steinberg*, 2010]; ii) adhesion into mucous nets formed by gelatinous

447 zooplankton, such as pteropods, and later settling [*Noji et al.*, 1997]; iii) inclusion into marine

448 snow via particle aggregation, which is enhanced by transparent exopolymer particles (TEP)

449 [*Passow*, 2002]. Passive sinking of fecal pellets could be a significant pathway for particle export

450 in the central Arctic where zooplankton exert a strong grazing pressure on algae, preventing their

451 biomass accumulation and sedimentation [*Olli et al.*, 2007]. Indeed, the copepod food demand

452 during our cruise was estimated to be similar to the in situ NPP rates [*David et al.*, 2015], leaving

453 a small fraction of algae available for direct export. Yet *Lalande et al.* [2014] estimated that only

454 up to 7.5% of the POC collected by traps at 25 m consisted of fecal pellets. Trap samples also

455 consisted of marine snow, debris, appendicularian houses, animal body parts and very sticky

456 material, even though their relative importance in POC content was not quantified (C. Lalande,

457 pers. comm.). Copepods clearly dominated the zooplankton community with regards to

458 abundance, whereas pteropods, ctenophores and appendicularians, which are prone to produce

459 mucous, represented less than 3-5% of the total zooplankton abundance either beneath the ice

460 [*David et al.*, 2015] or within the upper 50 m [*Ehrlich*, 2015]. However, ctenophores and

461 appendicularians dominated the under-ice zooplankton biomass at some stations, which could

462 have contributed notably to the export of mucous (C. David, pers. comm.). Moreover, sea-ice

463   algal aggregates of the centric diatom *Melosira arctica* and pennate diatoms were observed at all

464   the stations [*Fernández-Méndez et al.*, 2014]. They reached abundances up to 16 ind/m^2 and

465   extraordinary sizes (diameter mean: 2.1-4.1 cm), although they showed a highly patchy

466   distribution [*Katlein et al.*, 2014]. The aggregates were associated with mucous matrices that

467   increased their stickiness and, at the same time, their predisposition to aggregation [*Fernández-*

468   *Méndez et al.*, 2014]. Indeed, *Melosira arctica* was intercepted using sediment traps deployed at

469   25 m at some stations [*Lalande et al.*, 2014], confirming that it was part of the sinking pool.

470   Taken all together, sea-ice algal aggregates and zooplankton-derived material might have acted

471   as carriers of picoplankton cells from the ocean surface to depth (Figure 4b).

472   4.2 ^{210}Po/^{210}Pb

473   4.2.1 ^{210}Po and ^{210}Pb activities

474   ^{210}Po activities were lower than those of ^{210}Pb at every station in the upper 50-150 m,

475   indicating export driven by sinking particles, while excess ^{210}Po was observed at several depths

476   throughout the upper 400 m at stations 2 and 4, suggesting remineralization or particle

477   disaggregation (Figure 2). At stations 2 and 4 the integrated excess surpassed the integrated

478   deficit at 150 m and below, which can be explained by: i) a previous large export event that

479   occurred at the study sites, and/or ii) advection of waters that were enriched in ^{210}Po as

480   consequence of a previous export event [*Stewart et al.,* 2007]. Thus, the assumption of SS and/or

481   neglecting the advective term would have added uncertainty to our flux estimates of ^{210}Po. We

482   note that the ^{210}Po flux estimates are subject to be affected by NSS conditions or advection

483   transport processes to a larger extent than the ^{234}Th flux estimates due to the longer half-life of

484 ^{210}Po.

485   Very few studies have investigated the distribution of ^{210}Po and/or ^{210}Pb in the Arctic

486   water column [*Moore and Smith*, 1986; *Cochran et al.*, 1995a; *Smith and Ellis*, 1995; *Roberts et*

487   *al.*, 1997; *Smith et al.*, 2003; *Lepore et al.*, 2009; *Chen et al.*, 2012]. The ^{210}Pb and ^{210}Po

488   activities presented here are comparable to the wide activity range reported by those studies,

489   including shelf and basin areas.

490   In the Arctic, sea ice intercepts and accumulates atmospheric fluxes of chemical species,

491   such as ^{210}Pb, during its transit through the ocean [*Masqué et al.*, 2007; *Cámara-Mor et al.*,

492   2011] and, therefore, sea ice melting may increase ^{210}Pb activities in surface waters where that

493   occurs [*Roberts et al.*, 1997; *Masqué et al.,* 2007; *Chen et al.*, 2012]. One might wonder whether

494   sea ice melting may significantly impact the ^{210}Po and ^{210}Pb activities in seawater and, thus,

495   affect the use of the ^{210}Po proxy. Data on ^{210}Pb and ^{210}Po activities in entire sea-ice cores

496   collected during the same expedition (results not shown) show that the ^{210}Po/^{210}Pb ratios were

497   ≤0.5, indicating ^{210}Pb enrichment in sea ice, and consistent with the dominance of first-year ice

498   [*Masqué et al.,* 2007]. Given the inventories of both isotopes in sea-ice cores, even with

499   complete melting of sea ice, the ^{210}Po/^{210}Pb ratio in the upper 25 m of the water column would

500   have not changed or would have decreased as much as 10%. Since this change is relatively small,

501   we are confident that the principal cause of the ^{210}Po deficit in the upper water column was its

502   preferential removal via particle scavenging with respect to ^{210}Pb.

503   4.2.2 ^{210}Po export fluxes

504   The ^{210}Po export fluxes in the upper 150 m ranged from negligible to 8.2 dpm m^{-2} d^{-1},

505   averaging 3 ± 2 dpm m^{-2} d^{-1} (n = 28, Table 2). The fluxes obtained in this study are very low in

506   comparison to other studies conducted in other regions of the world ocean [*Shimmield et al.*,

507   1995; *Kim and Church*, 2001; *Friedrich and Rutgers van der Loeff*, 2002; *Murray et al.*, 2005;

508   *Stewart et al.*, 2007a; *Buesseler et al.*, 2008; *Verdeny et al.*, 2008; *Le Moigne et al.*, 2013a],

509   which reported fluxes from 5 to >100 dpm m^{-2} d^{-1}. However, the ^{210}Po fluxes were significant at

510   every station and at most of the investigated depths, in contrast to ^{234}Th fluxes, which were only

511   measurable at more than one depth at three stations (Table 2). Given the time scales of both

512   tracers, ^{210}Po would track particle export for the entire productive season, whereas ^{234}Th

513   distribution misses events that occurred >1 month before sampling. Thus, the more common

514   ^{210}Po depletion than that of ^{234}Th in the upper water column suggests that the magnitude of

515   particle export fluxes was more important before July/August 2012 than in the weeks prior to

516   and during the sampling (Figure 4).
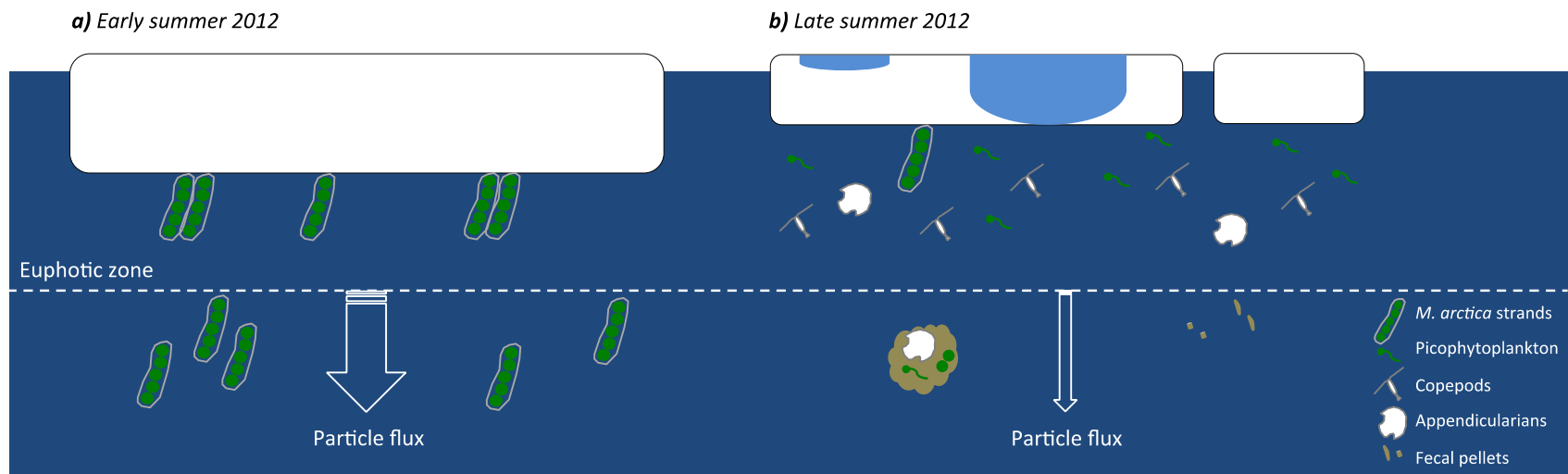
Figure 4: Scheme of the magnitude and composition of the particle fluxes in the central Arctic during the early (a) and late summer (b) in 2012 based on results from the present study and others [*Boetius et al.*, 2013; *Lalande et al.*, 2014; *David et al.*, 2015; *Fernández-Méndez et al.*, 2015] (see sections 4.1 and 4.2 for further details). Symbols are not drawn to scale.

521   *Boetius et al.* [2013] revealed the presence of vast deposits of sea-ice algal aggregates on

522   the seafloor at the majority of stations, which would have been exported from the ocean surface

523   earlier in the season, particularly before June at stations 4, 5 and 6 as suggested by the large body

524   size and fecundity of the deep-sea holothurians that fed on the algae. The aggregates were mainly

525   composed of *Melosira arctica* [*Boetius et al.,* 2013] that can form long strands hanging from the

526   ice bottom, sometimes up to 6 m long [*Melnikov and Bondarchuk,* 1987], allowing a rapid

527   sinking throughout the water column once detached. *Boetius et al.* [2013] estimated that algae

528   covered up to 10% of the seafloor by means of high-resolution pictures, accounting for a median

529   of 750 mmol C m^{-2} (± 50%). This POC inventory of algae was obtained by applying a cell

530   volume to carbon ratio (0.15 pg C μm^3) and a fixed thickness of the algal cover (0.01 m). This

531   supports the ^{210}Po evidence that the peak of export in the study area occurred in early summer

532   and sheds light on the composition of a major part of the sinking pool (Figure 4a). It was

533   estimated that diatoms were responsible for at least 45% of the total primary production in 2012

534   [*Boetius et al.,* 2013], indicating that the phytoplankton community varied over the productive

535   season, since diatoms did not contribute much to the Chl-a biomass during our cruise (~20%,

536   Table 1), when surface waters were silicate-depleted in most of the study area. Previous studies

537   with sediment traps also revealed that highest fluxes in the central Arctic occur mainly in June-

538   August [Fahl and Nötig 2007, Lalande et al. 2009].

539   4.2.3 Relationships with sea-ice conditions

540   There were significant relationships between the sea-ice conditions and the ^{210}Po-derived

541   fluxes. Sea-ice concentration was positively correlated with both ^{210}Po fluxes (p <0.01; ρ = 0.92;

542   n = 7) and ^{210}Po-derived POC fluxes (p <0.05; ρ = 0.91; n = 6) at 25 m. Indeed, the stations

543   located north of 87ºN and covered by multi-year ice (stations 7 and 8) showed the strongest

544   depletion of ^{210}Po within the upper 400 m (Figure 2), and the highest annual NPP rates (Table 1)

545   and seafloor algal coverage [*Boetius et al.,* 2013]. This suggests that primary production and

546   particle export were more important under heavy sea-ice conditions than under partially ice

547   covered stations and first-year ice, also suggesting that ^{210}Po tracked, to some extent, the massive

548   algal export that occurred earlier in 2012. On the contrary, at stations with heavy sea-ice

549   conditions we found the minimum in situ NPP rates (Table 1) and ^{234}Th in equilibrium with ^{238}U

550   throughout the upper water column (Figure 2), indicating low or negligible primary production

551   and particle export fluxes during the late summer.

552   The results presented here, combined with those from *Boetius et al.* [2013], show that the
553   central Arctic underwent significant changes during the productive season in terms of primary
554   production, phytoplankton composition and export fluxes during the record low of sea ice in
555   2012. This has implications for the use of ^{210}Po as a tracer: the depth distribution of total ^{210}Po
556   activity likely changed with time (NSS conditions) and the sinking material collected during the
557   survey probably did not cause the observed ^{210}Po depletion in the upper water column. Actually,
558   ^{210}Po activities in large particles collected at the time of sampling were inversely correlated with
559   ^{210}Po export fluxes at 25 m (p <0.05; ρ = -0.89; n = 6). The SS model would tend to smooth out
560   episodic export events that took place earlier in the season, and hence underestimate the mean
561   ^{210}Po fluxes and ^{210}Po-derived POC fluxes on a seasonal scale. On the other hand, we measured
562   C/Po ratios in particles that fall in the upper range of previous values (see review by *Verdeny et*
563   *al.* [2009]). *Stewart et al.* [2007] showed that C/Po ratios varied according to the sinking material
564   composition as follows: degraded material > fresh phytoplankton > fecal pellets. We also found
565   in some instances particulate ^{210}Po/^{210}Pb ratios below one (Table 3), which is inconsistent with
566   the ^{210}Po deficiency observed in surface waters. Particle types that may potentially explain low
567   ^{210}Po/^{210}Pb ratios could be: particles remineralized by chemical and biological processes [*Stewart*
568   *et al.*, 2007b], fecal material [*Stewart et al.*, 2005; *Rodriguez y Baena et al.*, 2007], picoplankton
569   aggregates [*Stewart et al.*, 2010], and substrates rich in transparent exopolymer particles
570   [*Quigley et al.*, 2002]. Overall, if the sinking pool responsible for ^{210}Po scavenging had different
571   C/Po ratios with respect to that collected at the sampling time, the ^{210}Po-derived POC fluxes
572   obtained in this study would not be fully representative of the fluxes that occurred in the
573   productive season in 2012.

574   4.3 Export efficiency

575   We have estimated the export efficiency by dividing the POC export fluxes derived from
576   ^{234}Th and ^{210}Po at 25 m (i.e. ~bottom of the euphotic zone) by different estimates of NPP that
577   encompass daily, weekly and annual time scales (Table 5).

Table 5: Export efficiency according to the ^{234}Th and ^{210}Po proxies estimated using different estimates of daily NPP (in situ, one and two weeks before sampling and annual new primary production; see text for further details).
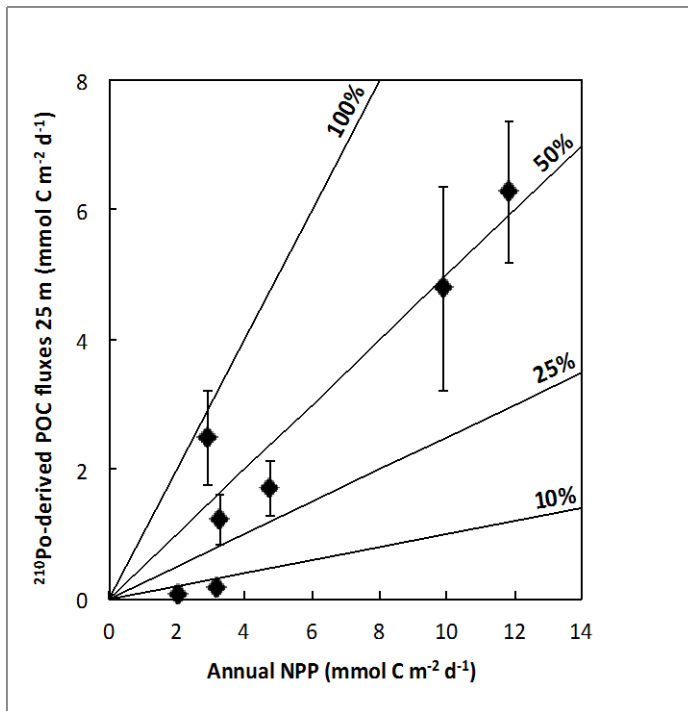
Station	Export efficiency (%)											
	In situ			One week			Two weeks			Annual		
Th proxy												
1[a]	>100			>100			>100			>100		
2[b]	*30*	*±*	*40*	*40*	*±*	*40*	*30*	*±*	*40*	*20*	*±*	*20*
3	0			0			0			0		
4	0			0			0			0		
5	90	±	20	>100			>100			77	±	18
6	80	±	20	100	±	30	80	±	20	60	±	17
7	*>100*			*>100*			*>100*			10	±	20
8	0			0			0			0		
9	nd			nd			nd			13	±	6
Po proxy												
1[a]	37	±	12	53	±	17	50	±	16	37	±	12
2[b]	64	±	16	74	±	19	67	±	17	36	±	9
3	*5*	*±*	*11*	*3*	*±*	*6*	*3*	*±*	*6*	*3*	*±*	*7*
4	>100			70	±	20	80	±	20	90	±	30
5	nd			nd			nd			nd		
6	8	±	3	9	±	4	8	±	3	6	±	2
7	>100			>100			>100			53	±	9
8	>100			>100			>100			48	±	16
9	nd			nd			nd			nd		

nd = no available data. The values in italics have relative uncertainties ≥100%. [a] POC fluxes used to estimate the export efficiency were measured at 15 m instead of 25 m. [b] POC fluxes used to estimate the export efficiency were measured at 50 m instead of 25 m.

582   Considering the in situ NPP rates, the export efficiency varied widely over the study site,

583   from 0 to >100%, averaging 50 ± 50% (n = 8) and 60 ± 40% (n = 7) for the [234]Th and [210]Po

584   proxies, respectively. The export efficiency calculated using the fluxes measured with sediment

585   traps [*Lalande et al.*, 2014] was >100% at 6 out of 8 stations. Export efficiencies over 100%

586   suggest that primary production that occurred earlier in the season contributed to the export

587   fluxes measured (i.e. temporal decoupling between production and export). In order to cover

588   longer time scales of NPP, we have also used estimates that integrate one and two weeks before

589   sampling and the entire productive season (see section 3.1.2). The increase in daily NPP

590   observed between the in-situ and the weekly estimates at stations 3, 4, 7 and 8, only changed

591   significantly the export efficiency at station 4 ([210]Po proxy), obtaining estimates of ~70% (Table

592   5). Export efficiencies over 100% were still observed in several instances, indicating that the lag

593   between production and export was longer than two weeks. On the contrary, the export

594   efficiencies decreased by about 40% applying the annual NPP estimates ([234]Th: 30 ± 40%, n = 9;

595   [210]Po: 40 ± 30%, n = 7) and were mostly below 100%, except for [234]Th at station 1. In contrast to

596   [234]Th, [210]Po fluxes and [210]Po-derived POC fluxes at 25 m showed a positive correlation with the

597   integrated deficits of nitrate found in the upper water column [*Fernández-Méndez et al.,* 2015] (p

598   <0.05; ρ = 0.83; n = 6), which are used to estimate the annual new NPP rates [e.g. *Codispoti et*

599   *al.*, 2013]. This confirms that the [210]Po proxy covered the productive season better than [234]Th,

600   and suggests that consumption of nitrate resulted in the increase in export production. Thus, the

601   [210]Po-derived POC fluxes and annual NPP estimates can be useful to assess the seasonal strength

602   of the biological pump, allowing to overcome the temporal decoupling between production and

603   export, which is especially long in Arctic waters conforming to a global biogeochemical model

604   [*Henson et al.*, 2015].

605   The export efficiency according to the annual NPP and the [210]Po-derived POC fluxes is

606   illustrated in Figure 5. Only two locations showed export efficiencies <10% (stations 3 and 6,

607   Table 5), which are those typically found in the world ocean [*Buesseler*, 1998]. Export

608   efficiencies >30% (average: 50 ± 20%, n = 5) were found at the other stations, which is in good

609   agreement with those reported by *Gustafsson and Andersson* [2012] in the Eurasian Basin

610   (average: 34 ± 8%, n = 3) and *Chen et al.* [2003] in the Canada Basin (26%, n = 1) applying

611   [234]Th-derived POC fluxes and in situ NPP rates. Our estimates are also similar to the [234]Th-

612   derived export efficiencies of ~30-40% reported for Chukchi shelf, slope and basin stations in

613   summer [*Moran et al.*, 2005; *Lepore et al.*, 2007]. Although only a limited set of observations of

614   export efficiency is available in the central Arctic, overall they point to high export efficiencies

615   as also indicated by *Henson et al.* [2015]. The assessment of the export efficiency in the central

616   Arctic deserves more attention to better understand its role as an export regime in a climate

617   change framework. Observations of strong aggregation and rapid algal falls in the central Arctic

618   [*Boetius et al.*, 2013; *Katlein et al.*, 2014] suggest a export system that works differently than in

619   most of the world ocean.

620

Figure 5: ^{210}Po-derived POC export fluxes at 25 m vs. annual new primary production reported in *Fernández-Méndez et al.* [2015]. Solid lines indicate the export efficiency.

5 Conclusions

624   We have used concurrently the ^{234}Th/^{238}U and ^{210}Po/^{210}Pb proxies to estimate POC fluxes in

625   the central Arctic during the record sea-ice minimum in 2012. The main findings of the present

626   work are:

627   1) ^{234}Th reveals that POC fluxes at the bottom of the euphotic zone were very low (2 ± 2

628   mmol C m^{-2} d^{-1}) in August/September, which is in good agreement with results obtained

629   using sediment traps (3 ± 3 mmol C m^{-2} d^{-1}) deployed at the same locations [*Lalande et*

630   *al.,* 2014]. The positive relationships found between prasinophytes_1 and ^{234}Th and

631   ^{234}Th-derived POC fluxes suggest that picoplankton contributed significantly to
632   downward fluxes in late summer.

633   2) In contrast to ^{234}Th, the upper water column was depleted in ^{210}Po over the entire study
634   area, indicating that particle export fluxes were higher before July/August than in the
635   weeks prior to and during the survey.

636   3) The positive relationships obtained between sea-ice concentration and ^{210}Po and ^{210}Po-
637   derived POC fluxes show that particle sinking was greater under heavy sea-ice conditions
638   than under partially ice covered areas. Further, the strongest ^{210}Po deficits in the water
639   column coincided with the highest seafloor coverage of algae reported by *Boetius et al.*
640   [2013], suggesting that ^{210}Po tracked, to some extent, the massive algal export that
641   occurred earlier in the season.

642   4) Although the POC fluxes were low, a large fraction of primary production (>30%) was
643   exported at the base of the euphotic zone in most of the study area, according to ^{210}Po-
644   derived POC fluxes and annual NPP estimates. Seasonal estimates of primary production
645   and export would be very helpful in characterizing the role of the Arctic biological pump
646   in the context of climate change.

647   We encourage future studies applying radionuclide proxies to consider NSS conditions and
648 follow the trend of C/Th and C/Po ratios with time to better constrain the POC fluxes in the
649 Arctic. Further, the simultaneous use of sediment traps would allow the determination of the
650 particle flux composition, which has been pointed out as a crucial factor shaping the biological
651 pump efficiency [e.g. *Mackinson et al.*, 2015; *Puigcorbé et al.*, 2015; *Roca-Martí et al.*, 2016].

References

666   Amacher, J., S. Neuer, and M. Lomas (2013), DNA-based molecular fingerprinting of eukaryotic
667   protists and cyanobacteria contributing to sinking particle flux at the Bermuda Atlantic
668   time-series study, *Deep Sea Res. Part II Top. Stud. Oceanogr.*, *93*, 71–83,
669   doi:10.1016/j.dsr2.2013.01.001.

670   Amiel, D., and J. K. Cochran (2008), Terrestrial and marine POC fluxes derived from 234Th
671   distributions and δ13C measurements on the Mackenzie Shelf, *J. Geophys. Res.*, *113*(C3),
672   1–19, doi:10.1029/2007JC004260.

673   Amiel, D., J. K. Cochran, and D. J. Hirschberg (2002), 234Th/238U disequilibrium as an
674   indicator of the seasonal export flux of particulate organic carbon in the North Water, *Deep
675   Sea Res. Part II Top. Stud. Oceanogr.*, *49*(22-23), 5191–5209, doi:10.1016/S0967-
676   0645(02)00185-6.

677   Anderson, L. G., and R. W. Macdonald (2015), Observing the Arctic Ocean carbon cycle in a
678   changing environment, *Polar Res.*, *34*(26891), doi:10.3402/polar.v34.26891.

679   Anderson, L. G., E. Peter Jones, and J. H. Swift (2003), Export production in the central Arctic
680   Ocean evaluated from phosphate deficits, *J. Geophys. Res. Ocean.*, *108*(C6), 6 pp.,
681   doi:10.1029/2001JC001057.

682   Arrigo, K. R., and G. L. van Dijken (2015), Continued increases in Arctic Ocean primary
683   production, *Prog. Oceanogr.*, *136*, 60–70, doi:10.1016/j.pocean.2015.05.002.

684   Arrigo, K. R. et al. (2012), Massive phytoplankton blooms under Arctic sea ice, *Science*,
685   *336*(6087), 1408, doi:10.1126/science.1215065.

686   Barlow, R. ., D. . Cummings, and S. . Gibb (1997), Improved resolution of mono- and divinyl
687   chlorophylls a and b and zeaxanthin and lutein in phytoplankton extracts using reverse
688   phase C-8 HPLC, *Mar. Ecol. Ser.*, *161*, 303–307, doi:10.3354/meps161303.

689   Baskaran, M., P. W. Swarzenski, and D. Porcelli (2003), Role of colloidal material in the
690   removal of 234Th in the Canada basin of the Arctic Ocean, *Deep Sea Res. Part I Oceanogr.*
691   *Res. Pap.*, *50*(10-11), 1353–1373, doi:10.1016/S0967-0637(03)00140-7.

692   Bidigare, R. R. (1991), Analysis of Algal Chlorophylls and Carotenoids, in *Marine Particles:*
693   *Analysis and Characterization*, edited by D. C. Hurd and D. W. Spencer, pp. 119–123,
694   American Geophysical Union, Washington, D. C.

695   Boetius, A. (2013), *The expedition of the research vessel "Polarstern" to the Arctic in 2012*
696   *(ARK-XXVII/3). Reports on polar and marine research 663*, Bremerhaven.

697   Boetius, A. et al. (2013), Export of algal biomass from the melting Arctic sea ice, *Science*,
698   *339*(6126), 1430–1432, doi:10.1126/science.1231346.

699   Booth, B. C., and R. A. Horner (1997), Microalgae on the arctic ocean section, 1994: species

abundance and biomass, *Deep Sea Res. Part II Top. Stud. Oceanogr.*, *44*(8), 1607–1622, doi:10.1016/S0967-0645(97)00057-X.

Buesseler, K. O. (1998), The decoupling of production and particulate export in the surface ocean, *Global Biogeochem. Cycles*, *12*(2), 297–310, doi:10.1029/97GB03366.

Buesseler, K. O., and P. Boyd (2009), Shedding light on processes that control particle export and flux attenuation in the twilight zone of the open ocean, *Limnol. Oceanogr.*, *54*(4), 1210–1232, doi:10.4319/lo.2009.54.4.1210.

Buesseler, K. O., M. P. Bacon, J. K. Cochran, and H. D. Livingston (1992), Carbon and nitrogen export during the JGOFS North Atlantic Bloom experiment estimated from 234Th: 238U disequilibria, *Deep Sea Res. Part A. Oceanogr. Res. Pap.*, *39*(7-8), 1115–1137, doi:10.1016/0198-0149(92)90060-7.

Buesseler, K. O., C. Benitez-Nelson, M. M. Rutgers van der Loeff, J. Andrews, L. Ball, G. Crossin, and M. A. Charette (2001), An intercomparison of small- and large-volume techniques for thorium-234 in seawater, *Mar. Chem.*, *74*(1), 15–28, doi:10.1016/S0304-4203(00)00092-X.

Buesseler, K. O., C. Lamborg, P. Cai, R. Escoube, R. Johnson, S. Pike, P. Masque, D. McGillicuddy, and E. Verdeny (2008), Particle fluxes associated with mesoscale eddies in the Sargasso Sea, *Deep Sea Res. Part II Top. Stud. Oceanogr.*, *55*(10-13), 1426–1444, doi:10.1016/j.dsr2.2008.02.007.

Cai, P., M. M. Rutgers van der Loeff, I. Stimac, E.-M. Nöthig, K. Lepore, and S. B. Moran (2010), Low export flux of particulate organic carbon in the central Arctic Ocean as revealed by 234Th:238U disequilibrium, *J. Geophys. Res.*, *115*(C10037), 1–21, doi:10.1029/2009JC005595.

Cámara-Mor, P., P. Masqué, J. Garcia-Orellana, S. Kern, J. K. Cochran, and C. Hanfland (2011), Interception of atmospheric fluxes by Arctic sea ice: Evidence from cosmogenic 7Be, *J. Geophys. Res. Ocean.*, *116*(C12041), 1–10, doi:10.1029/2010JC006847.

Chen, M., Y. Huang, P. Cai, and L. Guo (2003), Particulate Organic Carbon Export Fluxes in The Canada Basin and Bering Sea as Derived from 234Th/238U Disequilibria, *ARCTIC*, *56*(1), 32–44, doi:10.14430/arctic600.

Chen, M., Q. Ma, L. Guo, Y. Qiu, Y. Li, and W. Yang (2012), Importance of lateral transport processes to 210Pb budget in the eastern Chukchi Sea during summer 2003, *Deep Sea Res. Part II Top. Stud. Oceanogr.*, *81-84*, 53–62, doi:10.1016/j.dsr2.2012.03.011.

Cochran, J. K., D. J. Hirschberg, H. D. Livingston, K. O. Buesseler, and R. M. Key (1995a), Natural and anthropogenic radionuclide distributions in the Nansen Basin, Artic Ocean: Scavenging rates and circulation timescales, *Deep Sea Res. Part II Top. Stud. Oceanogr.*, *42*(6), 1495–1517, doi:10.1016/0967-0645(95)00051-8.

Cochran, J. K., C. Barnes, D. Achman, and D. J. Hirschberg (1995b), Thorium-234/Uranium-238 disequilibrium as an indicator of scavenging rates and particulate organic carbon fluxes in the Northeast Water Polynya, Greenland, *J. Geophys. Res.*, *100*(C3), 4399–4410, doi:10.1029/94JC01954.

Codispoti, L. A. A., V. Kelly, A. Thessen, P. Matrai, S. Suttles, V. Hill, M. Steele, and B. Light (2013), Synthesis of primary production in the Arctic Ocean: III. Nitrate and phosphate

742   based estimates of net community production, *Prog. Oceanogr.*, *110*, 126–150,
743   doi:10.1016/j.pocean.2012.11.006.

744 Coppola, L., M. Roy-Barman, P. Wassmann, S. Mulsow, and C. Jeandel (2002), Calibration of
745   sediment traps and particulate organic carbon export using 234Th in the Barents Sea, *Mar.*
746   *Chem.*, *80*(1), 11–26, doi:10.1016/S0304-4203(02)00071-3.

747 David, C., B. Lange, B. Rabe, and H. Flores (2015), Community structure of under-ice fauna in
748   the Eurasian central Arctic Ocean in relation to environmental properties of sea-ice habitats,
749   *Mar. Ecol. Prog. Ser.*, *522*, 15–32.

750 Durkin, C. A., M. L. Estapa, and K. O. Buesseler (2015), Observations of carbon export by small
751   sinking particles in the upper mesopelagic, *Mar. Chem.*, *175*, 72–81,
752   doi:10.1016/j.marchem.2015.02.011.

753 Ehrlich, J. (2015), Diversity and distribution of high-Arctic zooplankton in the Eurasian Basin in
754   late summer 2012, Master thesis, University of Hamburg, Alfred Wegener Institute.

755 Fahl, K., and E.-M. Nöthig (2007), Lithogenic and biogenic particle fluxes on the Lomonosov
756   Ridge (central Arctic Ocean) and their relevance for sediment accumulation: Vertical vs.
757   lateral transport, *Deep Sea Res. Part I Oceanogr. Res. Pap.*, *54*(8), 1256–1272,
758   doi:10.1016/j.dsr.2007.04.014.

759 Falkowski, P. G., R. T. Barber, and V. Smetacek (1998), Biogeochemical Controls and
760   Feedbacks on Ocean Primary Production, *Science*, *281*(5374), 200–206,
761   doi:10.1126/science.281.5374.200.

762 Fernández-Méndez, M., F. Wenzhöfer, I. Peeken, H. L. Sørensen, R. N. Glud, and A. Boetius
763   (2014), Composition, buoyancy regulation and fate of ice algal aggregates in the Central
764   Arctic Ocean., *PLoS One*, *9*(9), 13 pp., doi:10.1371/journal.pone.0107452.

765 Fernández-Méndez, M., C. Katlein, B. Rabe, M. Nicolaus, I. Peeken, K. Bakker, H. Flores, and
766   A. Boetius (2015), Photosynthetic production in the central Arctic Ocean during the record
767   sea-ice minimum in 2012, *Biogeosciences*, *12*(11), 3525–3549, doi:10.5194/bg-12-3525-
768   2015.

769 Fleer, A. P., and M. P. Bacon (1984), Determination of 210Pb and 210Po in seawater and marine
770   particulate matter, *Nucl. Instruments Methods Phys. Res.*, *223*(2-3), 243–249,
771   doi:10.1016/0167-5087(84)90655-0.

772 Flynn, W. W. (1968), The determination of low levels of polonium-210 in environmental
773   materials., *Anal. Chim. Acta*, *43*(2), 221–227.

774 Fortier, M., L. Fortier, C. Michiel, and L. Legendre (2002), Climatic and biological forcing of
775   the vertical flux of biogenic particles under seasonal Arctic sea ice, *Mar. Ecol. Prog. Ser.*,
776   *225*, 1–16, doi:10.3354/meps225001.

777 Le Fouest, V., M. Babin, and J.-É. Tremblay (2013), The fate of riverine nutrients on Arctic
778   shelves, *Biogeosciences*, *10*, 3661– 3677, doi:10.5194/bg-10-3661-2013.

779 Friedrich, J., and M. M. Rutgers van der Loeff (2002), A two-tracer (210Po–234Th) approach to
780   distinguish organic carbon and biogenic silica export flux in the Antarctic Circumpolar
781   Current, *Deep Sea Res. Part I Oceanogr. Res. Pap.*, *49*(1), 101–120, doi:10.1016/S0967-
782   0637(01)00045-0.

783 Gosselin, M., M. Levasseur, P. A. Wheeler, R. A. Horner, and B. C. Booth (1997), New
784   measurements of phytoplankton and ice algal production in the Arctic Ocean, *Deep Sea*
785   *Res. Part II Top. Stud. Oceanogr.*, *44*(8), 1623–1644, doi:10.1016/S0967-0645(97)00054-4.

786 Gradinger, R., C. Friedrich, and M. Spindler (1999), Abundance, biomass and composition of the
787   sea ice biota of the Greenland Sea pack ice, *Deep Sea Res. Part IITopical Stud. Oceanogr.*,
788   *46*(6-7), 1457–1472, doi:10.1016/S0967-0645(99)00030-2.

789 Gruber, N. et al. (2009), Oceanic sources, sinks, and transport of atmospheric CO2, *Global*
790   *Biogeochem. Cycles*, *23*(1), 1–21, doi:10.1029/2008GB003349.

791 Gustafsson, Ö., and P. S. Andersson (2012), 234Th-derived surface export fluxes of POC from
792   the Northern Barents Sea and the Eurasian sector of the Central Arctic Ocean, *Deep Sea*
793   *Res. Part I Oceanogr. Res. Pap.*, *68*, 1–11, doi:10.1016/j.dsr.2012.05.014.

794 Haas, C., A. Pfaffling, S. Hendricks, L. Rabenstein, J.-L. Etienne, and I. Rigor (2008), Reduced
795   ice thickness in Arctic Transpolar Drift favors rapid ice retreat, *Geophys. Res. Lett.*,
796   *35*(L17501), 1–5, doi:10.1029/2008GL034457.

797 Henson, S. A., A. Yool, and R. Sanders (2015), Variability in efficiency of particulate organic
798   carbon export: A model study, *Global Biogeochem. Cycles*, *29*(1), 33–45,
799   doi:10.1002/2014GB004965.

800 Higgins, H. W., S. W. Wright, and L. Schlüter (2011), Quantitative interpretation of
801   chemotaxonomic pigment data, in *Phytoplankton Pigments. Characterization,*
802   *Chemotaxonomy and Applications in Oceanography*, edited by S. Roy, C. Llewellyn, E. S.
803   Egeland, and G. Johnsen, pp. 257–313, Cambridge University Press, Cambridge.

804 Hirata, T. et al. (2011), Synoptic relationships between surface Chlorophyll-*a* and diagnostic
805   pigments specific to phytoplankton functional types, *Biogeosciences*, *8*(2), 311–327,
806   doi:10.5194/bg-8-311-2011.

807 Honjo, S., R. A. Krishfield, T. I. Eglinton, S. J. Manganini, J. N. Kemp, K. Doherty, J. Hwang,
808   T. K. McKee, and T. Takizawa (2010), Biological pump processes in the cryopelagic and
809   hemipelagic Arctic Ocean: Canada Basin and Chukchi Rise, *Prog. Oceanogr.*, *85*(3-4),
810   137–170, doi:10.1016/j.pocean.2010.02.009.

811 Jeffrey, S. W., R. F. C. Mantoura, and T. Bjørnland (1997), Data for the identification of 47 key
812   phytoplankton pigments, in *Phytoplankton pigments in oceanography: guidelines to modern*
813   *methods*, edited by S. W. Jeffrey, R. F. C. Mantoura, and S. W. Wright, pp. 449–559,
814   Cambridge University Press, Paris.

815 Katlein, C., M. Fernández-Méndez, F. Wenzhöfer, and M. Nicolaus (2014), Distribution of algal
816   aggregates under summer sea ice in the Central Arctic, *Polar Biol.*, *38*(5), 719–731,
817   doi:10.1007/s00300-014-1634-3.

818 Kilias, E., C. Wolf, E.-M. Nöthig, I. Peeken, and K. Metfies (2013), Protist distribution in the
819   Western Fram Strait in summer 2010 based on 454-pyrosequencing of 18S rDNA, edited by
820   T. Mock, *J. Phycol.*, *49*(5), 996–1010, doi:10.1111/jpy.12109.

821 Kim, G., and T. M. Church (2001), Seasonal biogeochemical fluxes of 234 Th and 210 Po in the
822   Upper Sargasso Sea: Influence from atmospheric iron deposition, *Global Biogeochem.*
823   *Cycles*, *15*(3), 651–661, doi:10.1029/2000GB001313.

824 Knap, A., A. Michaels, A. Close, H. Ducklow, and A. Dickson (1996), *Protocols for the Joint*

825   *Global Ocean Flux Study (JGOFS) Core Measurements. JGOFS Report Nr. 19.*

826   Lalande, C., K. Lepore, L. W. Cooper, J. M. Grebmeier, and S. B. Moran (2007), Export fluxes
827   of particulate organic carbon in the Chukchi Sea: A comparative study using 234Th/238U
828   disequilibria and drifting sediment traps, *Mar. Chem.*, *103*(1-2), 185–196,
829   doi:10.1016/j.marchem.2006.07.004.

830   Lalande, C., S. B. Moran, P. Wassmann, J. M. Grebmeier, and L. W. Cooper (2008), 234Th-
831   derived particulate organic carbon fluxes in the northern Barents Sea with comparison to
832   drifting sediment trap fluxes, *J. Mar. Syst.*, *73*(1-2), 103–113,
833   doi:10.1016/j.jmarsys.2007.09.004.

834   Lalande, C., A. Forest, D. G. Barber, Y. Gratton, and L. Fortier (2009), Variability in the annual
835   cycle of vertical particulate organic carbon export on Arctic shelves: Contrasting the Laptev
836   Sea, Northern Baffin Bay and the Beaufort Sea, *Cont. Shelf Res.*, *29*(17), 2157–2165,
837   doi:10.1016/j.csr.2009.08.009.

838   Lalande, C., E.-M. Nöthig, R. Somavilla, E. Bauerfeind, V. Shevchenko, and Y. Okolodkov
839   (2014), Variability in under-ice export fluxes of biogenic matter in the Arctic Ocean, *Global
840   Biogeochem. Cycles*, *28*(5), 571–583, doi:10.1002/2013GB004735.

841   Lee, S. H., D. Stockwell, and T. E. Whitledge (2010), Uptake rates of dissolved inorganic carbon
842   and nitrogen by under-ice phytoplankton in the Canada Basin in summer 2005, *Polar Biol.*,
843   *33*(8), 1027–1036, doi:10.1007/s00300-010-0781-4.

844   Lepore, K. et al. (2007), Seasonal and interannual changes in particulate organic carbon export
845   and deposition in the Chukchi Sea, *J. Geophys. Res.*, *112*(C10024), 1–14,
846   doi:10.1029/2006JC003555.

847   Lepore, K., S. B. Moran, and J. N. Smith (2009), 210Pb as a tracer of shelf–basin transport and
848   sediment focusing in the Chukchi Sea, *Deep Sea Res. Part II Top. Stud. Oceanogr.*, *56*(17),
849   1305–1315, doi:10.1016/j.dsr2.2008.10.021.

850   Li, W. K. W., F. A. McLaughlin, C. Lovejoy, and E. C. Carmack (2009), Smallest algae thrive as
851   the Arctic Ocean freshens., *Science*, *326*(5952), 539, doi:10.1126/science.1179798.

852   Lomas, M. W., and S. B. Moran (2011), Evidence for aggregation and export of cyanobacteria
853   and nano-eukaryotes from the Sargasso Sea euphotic zone, *Biogeosciences*, *8*(1), 203–216,
854   doi:10.5194/bg-8-203-2011.

855   Lovejoy, C., W. F. Vincent, S. Bonilla, S. Roy, M.-J. Martineau, R. Terrado, M. Potvin, R.
856   Massana, and C. Pedrós-Alió (2007), Distribution, phylogeny, and growth of cold-adapted
857   picoprasinophytes in Arctic seas, *J. Phycol.*, *43*(1), 78–89, doi:10.1111/j.1529-
858   8817.2006.00310.x.

859   Ma, Q., M. Chen, Y. Qiu, and Y. Li (2005), Regional estimates of POC export flux derived from
860   thorium-234 in the western Arctic Ocean, *Acta Oceanol. Sin.*, *24*(6), 97–108.

861   Mackey, M., D. Mackey, H. Higgins, and S. Wright (1996), CHEMTAX - a program for
862   estimating class abundances from chemical markers: application to HPLC measurements of
863   phytoplankton, *Mar. Ecol. Ser.*, *144*, 265–283.

864   Mackinson, B. L., S. B. Moran, M. W. Lomas, G. M. Stewart, and R. P. Kelly (2015), Estimates
865   of micro-, nano-, and picoplankton contributions to particle export in the northeast Pacific,
866   *Biogeosciences*, *12*(11), 3429–3446, doi:10.5194/bg-12-3429-2015.

867 Masqué, P., J. K. Cochran, D. J. Hirschberg, D. Dethleff, D. Hebbeln, A. Winkler, and S.
868   Pfirman (2007), Radionuclides in Arctic sea ice: Tracers of sources, fates and ice transit
869   time scales, *Deep Sea Res. Part I Oceanogr. Res. Pap.*, *54*(8), 1289–1310,
870   doi:10.1016/j.dsr.2007.04.016.

871 Matrai, P. A., E. Olson, S. Suttles, V. Hill, L. A. Codispoti, B. Light, and M. Steele (2013),
872   Synthesis of primary production in the Arctic Ocean: I. Surface waters, 1954–2007, *Prog.*
873   *Oceanogr.*, *110*, 93–106, doi:10.1016/j.pocean.2012.11.004.

874 Melnikov, I. A., and L. L. Bondarchuk (1987), Ecology of mass accumulations of colonial
875   diatom algae under drifting Arctic ice, *Oceanology*, *27*(2), 233–236,
876   doi:10.1594/PANGAEA.756627.

877 Metfies, K., W.-J. von Appen, E. Kilias, A. Nicolaus, and E.-M. Nöthig (2016), Biogeography
878   and Photosynthetic Biomass of Arctic Marine Pico-Eukaroytes during Summer of the
879   Record Sea Ice Minimum 2012, *PLoS One*, *11*(2), 20 pp.,
880   doi:10.1371/journal.pone.0148512.

881 Le Moigne, F. A. C., M. Villa-Alfageme, R. J. Sanders, C. Marsay, S. Henson, and R. García-
882   Tenorio (2013a), Export of organic carbon and biominerals derived from 234Th and 210Po
883   at the Porcupine Abyssal Plain, *Deep Sea Res. Part I Oceanogr. Res. Pap.*, *72*, 88–101,
884   doi:10.1016/j.dsr.2012.10.010.

885 Le Moigne, F. A. C., S. A. Henson, R. J. Sanders, and E. Madsen (2013b), Global database of
886   surface ocean particulate organic carbon export fluxes diagnosed from the [234]Th technique,
887   *Earth Syst. Sci. Data*, *5*(2), 295–304, doi:10.5194/essd-5-295-2013.

888 Le Moigne, F. A. C. et al. (2015), Carbon export efficiency and phytoplankton community
889   composition in the Atlantic sector of the Arctic Ocean, *J. Geophys. Res. Ocean.*, *120*(6),
890   3896–3912, doi:10.1002/2015JC010700.

891 Moore, R. M., and J. N. Smith (1986), Disequilibria between 226Ra, 210Pb and 210Po in the
892   Arctic Ocean and the implications for chemical modification of the Pacific water inflow,
893   *Earth Planet. Sci. Lett.*, *77*(3-4), 285–292, doi:10.1016/0012-821X(86)90140-8.

894 Moran, S. B., and J. N. Smith (2000), 234Th as a tracer of scavenging and particle export in the
895   Beaufort Sea, *Cont. Shelf Res.*, *20*(2), 153–167, doi:10.1016/S0278-4343(99)00065-5.

896 Moran, S. B., K. M. Ellis, and J. N. Smith (1997), 234Th/238U disequilibrium in the central
897   Arctic Ocean: implications for particulate organic carbon export, *Deep Sea Res. Part II Top.*
898   *Stud. Oceanogr.*, *44*(8), 1593–1606, doi:10.1016/S0967-0645(97)00049-0.

899 Moran, S. B. et al. (2005), Seasonal changes in POC export flux in the Chukchi Sea and
900   implications for water column-benthic coupling in Arctic shelves, *Deep Sea Res. Part II*
901   *Top. Stud. Oceanogr.*, *52*(24-26), 3427–3451, doi:10.1016/j.dsr2.2005.09.011.

902 Murray, J. W., B. Paul, J. P. Dunne, and T. Chapin (2005), 234Th, 210Pb, 210Po and stable Pb
903   in the central equatorial Pacific: Tracers for particle cycling, *Deep Sea Res. Part I*
904   *Oceanogr. Res. Pap.*, *52*(11), 2109–2139, doi:10.1016/j.dsr.2005.06.016.

905 Nicolaus, M., C. Katlein, J. Maslanik, and S. Hendricks (2012), Changes in Arctic sea ice result
906   in increasing light transmittance and absorption, *Geophys. Res. Lett.*, *39*(L24501), 1–6,
907   doi:10.1029/2012GL053738.

908 Noji, T. T., U. V. Bathmann, B. von Bodungen, M. Voss, A. Antia, M. Krumbholz, B. Klein, I.

Peeken, C. I.-M. Noji, and F. Rey (1997), Clearance of picoplankton-sized particles and formation of rapidly sinking aggregates by the pteropod, Limacina retroversa, *J. Plankton Res.*, *19*(7), 863–875, doi:10.1093/plankt/19.7.863.

Not, C., K. Brown, B. Ghaleb, and C. Hillaire-Marcel (2012), Conservative behavior of uranium vs. salinity in Arctic sea ice and brine, *Mar. Chem.*, *130-131*, 33–39, doi:10.1016/j.marchem.2011.12.005.

Olli, K. et al. (2007), The fate of production in the central Arctic Ocean – top–down regulation by zooplankton expatriates?, *Prog. Oceanogr.*, *72*(1), 84–113, doi:10.1016/j.pocean.2006.08.002.

Overland, J. E., and M. Wang (2013), When will the summer Arctic be nearly sea ice free?, *Geophys. Res. Lett.*, *40*(10), 2097–2101, doi:10.1002/grl.50316.

Owens, S. A., K. O. Buesseler, and K. W. W. Sims (2011), Re-evaluating the 238U-salinity relationship in seawater: Implications for the 238U–234Th disequilibrium method, *Mar. Chem.*, *127*(1-4), 31–39, doi:10.1016/j.marchem.2011.07.005.

Parkinson, C. L., and J. C. Comiso (2013), On the 2012 record low Arctic sea ice cover: Combined impact of preconditioning and an August storm, *Geophys. Res. Lett.*, *40*(7), 1356–1361, doi:10.1002/grl.50349.

Passow, U. (2002), Transparent exopolymer particles (TEP) in aquatic environments, *Prog. Oceanogr.*, *55*(3-4), 287–333, doi:10.1016/S0079-6611(02)00138-6.

Pike, S., K. Buesseler, J. Andrews, and N. Savoye (2005), Quantification of 234Th recovery in small volume sea water samples by inductively coupled plasma-mass spectrometry, *J. Radioanal. Nucl. Chem.*, *263*(2), 355–360, doi:10.1007/s10967-005-0594-z.

Puigcorbé, V., C. R. Benitez-Nelson, P. Masqué, E. Verdeny, A. E. White, B. N. Popp, F. G. Prahl, and P. J. Lam (2015), Small phytoplankton drive high summertime carbon and nutrient export in the Gulf of California and Eastern Tropical North Pacific, *Global Biogeochem. Cycles*, *29*(8), 1309–1332, doi:10.1002/2015GB005134.

Quigley, M. S., P. H. Santschi, C.-C. Hung, L. Guo, and B. D. Honeyman (2002), Importance of acid polysaccharides for 234Th complexation to marine organic matter, *Limnol. Oceanogr.*, *47*(2), 367–377, doi:10.4319/lo.2002.47.2.0367.

Richardson, T. L., and G. A. Jackson (2007), Small phytoplankton and carbon export from the surface ocean, *Science*, *315*(5813), 838–840, doi:10.1126/science.1133471.

Rigaud, S., V. Puigcorbé, P. Cámara-Mor, N. Casacuberta, M. Roca-Martí, J. Garcia-Orellana, C. R. Benitez-Nelson, P. Masqué, and T. Church (2013), A methods assessment and recommendations for improving calculations and reducing uncertainties in the determination of 210Po and 210Pb activities in seawater, *Limnol. Oceanogr. Methods*, *11*(10), 561–571, doi:10.4319/lom.2013.11.561.

Roberts, K. A., J. K. Cochran, and C. Barnes (1997), 210Pb and 239,240Pu in the Northeast Water Polynya, Greenland: particle dynamics and sediment mixing rates, *J. Mar. Syst.*, *10*(1-4), 401–413, doi:10.1016/S0924-7963(96)00061-9.

Roca-Martí, M., V. Puigcorbé, M. H. Iversen, M. M. Rutgers van der Loeff, C. Klaas, W. Cheah, A. Bracher, and P. Masqué (2016), High particulate organic carbon export during the decline of a vast diatom bloom in the Atlantic sector of the Southern Ocean, *Deep Sea Res.*

951   *Part II Top. Stud. Oceanogr.*, doi:10.1016/j.dsr2.2015.12.007.

952   Rodriguez y Baena, A. M., S. W. Fowler, and J. C. Miquel (2007), Particulate organic carbon :
953   natural radionuclide ratios in zooplankton and their freshly produced fecal pellets from the
954   NW Mediterranean (MedFlux 2005), *Limnol. Oceanogr.*, *52*(3), 966–974,
955   doi:10.4319/lo.2007.52.3.0966.

956   Rudels, B. (2009), Arctic Ocean Circulation, in *Ocean Currents: A Derivative of the*
957   *Encyclopedia of Ocean Sciences*, edited by J. H. Steele, S. A. Thorpe, and K. K. Turekian,
958   pp. 211–225, Academic Press, London.

959   Rutgers van der Loeff, M. M. et al. (2006), A review of present techniques and methodological
960   advances in analyzing 234Th in aquatic systems, *Mar. Chem.*, *100*(3-4), 190–212,
961   doi:10.1016/j.marchem.2005.10.012.

962   Savoye, N., C. Benitez-Nelson, A. B. Burd, J. K. Cochran, M. Charette, K. O. Buesseler, G. A.
963   Jackson, M. Roy-Barman, S. Schmidt, and M. Elskens (2006), 234Th sorption and export
964   models in the water column: A review, *Mar. Chem.*, *100*(3-4), 234–249,
965   doi:10.1016/j.marchem.2005.10.014.

966   Shaw, W. J., T. P. Stanton, M. G. McPhee, J. H. Morison, and D. G. Martinson (2009), Role of
967   the upper ocean in the energy budget of Arctic sea ice during SHEBA, *J. Geophys. Res.*,
968   *114*(C6), C06012, doi:10.1029/2008JC004991.

969   Sherr, E. B., B. F. Sherr, P. A. Wheeler, and K. Thompson (2003), Temporal and spatial
970   variation in stocks of autotrophic and heterotrophic microbes in the upper water column of
971   the central Arctic Ocean, *Deep Sea Res. Part I Oceanogr. Res. Pap.*, *50*(5), 557–571,
972   doi:10.1016/S0967-0637(03)00031-1.

973   Shimmield, G. B., G. D. Ritchie, and T. W. Fileman (1995), The impact of marginal ice zone
974   processes on the distribution of 210Pb, 210Po and 234Th and implications for new
975   production in the Bellingshausen Sea, Antarctica, *Deep Sea Res. Part II Top. Stud.*
976   *Oceanogr.*, *42*(4-5), 1313–1335, doi:10.1016/0967-0645(95)00071-W.

977   Smith, J. ., S. . Moran, and R. . Macdonald (2003), Shelf–basin interactions in the Arctic Ocean
978   based on 210Pb and Ra isotope tracer distributions, *Deep Sea Res. Part I Oceanogr. Res.*
979   *Pap.*, *50*(3), 397–416, doi:10.1016/S0967-0637(02)00166-8.

980   Smith, J. N., and K. M. Ellis (1995), Radionuclide tracer profiles at the CESAR Ice Station and
981   Canadian Ice Island in the western Arctic Ocean, *Deep Sea Res. Part II Top. Stud.*
982   *Oceanogr.*, *42*(6), 1449–1470, doi:10.1016/0967-0645(95)00049-6.

983   Smith, R. E. H., M. Gosselin, and S. Taguchi (1997), The influence of major inorganic nutrients
984   on the growth and physiology of high arctic ice algae, *J. Mar. Syst.*, *11*(1-2), 63–70,
985   doi:10.1016/S0924-7963(96)00028-0.

986   Spreen, G., L. Kaleschke, and G. Heygster (2008), Sea ice remote sensing using AMSR-E 89-
987   GHz channels, *J. Geophys. Res. Ocean.*, *113*(C2), C02S03, doi:10.1029/2005JC003384.

988   Steemann Nielsen, E. (1952), The use of radio-active carbon (C14) for measuring organic
989   production in the sea, *J. Cons. Int. Explor. Mer.*, *18*(2), 117–140,
990   doi:10.1093/icesjms/18.2.117.

991   Stewart, G., S. Fowler, J. L. Teyssié, O. Cotret, J. K. Cochran, and N. S. Fisher (2005),
992   Contrasting transfer of polonium-210 and lead-210 across three trophic levels in marine

993   plankton, *Mar. Ecol. Prog. Ser.*, *290*, 27–33.

994   Stewart, G., J. K. Cochran, J. C. Miquel, P. Masqué, J. Szlosek, A. M. Rodriguez y Baena, S. W.
995   Fowler, B. Gasser, and D. J. Hirschberg (2007a), Comparing POC export from 234Th/238U
996   and 210Po/210Pb disequilibria with estimates from sediment traps in the northwest
997   Mediterranean, *Deep Sea Res. Part I Oceanogr. Res. Pap.*, *54*(9), 1549–1570,
998   doi:10.1016/j.dsr.2007.06.005.

999   Stewart, G., J. Kirk Cochran, J. Xue, C. Lee, S. G. Wakeham, R. A. Armstrong, P. Masqué, and
1000   J. Carlos Miquel (2007b), Exploring the connection between 210Po and organic matter in
1001   the northwestern Mediterranean, *Deep Sea Res. Part I Oceanogr. Res. Pap.*, *54*(3), 415–
1002   427, doi:10.1016/j.dsr.2006.12.006.

1003   Stewart, G., S. B. Moran, M. W. Lomas, and R. P. Kelly (2011), Direct comparison of 210Po,
1004   234Th and POC particle-size distributions and export fluxes at the Bermuda Atlantic Time-
1005   series Study (BATS) site., *J. Environ. Radioact.*, *102*(5), 479–489,
1006   doi:10.1016/j.jenvrad.2010.09.011.

1007   Stewart, G. M., S. Bradley Moran, and M. W. Lomas (2010), Seasonal POC fluxes at BATS
1008   estimated from 210Po deficits, *Deep Sea Res. Part I Oceanogr. Res. Pap.*, *57*(1), 113–124,
1009   doi:10.1016/j.dsr.2009.09.007.

1010   Taylor, B. B., E. Torrecilla, A. Bernhardt, M. H. Taylor, I. Peeken, R. Röttgers, J. Piera, and A.
1011   Bracher (2011), Bio-optical provinces in the eastern Atlantic Ocean and their
1012   biogeographical relevance, *Biogeosciences Discuss.*, *8*, 7165–7219.

1013   Tremblay, J.-É., L. G. Anderson, P. Matrai, P. Coupel, S. Bélanger, C. Michel, and M. Reigstad
1014   (2015), Global and regional drivers of nutrient supply, primary production and CO2
1015   drawdown in the changing Arctic Ocean, *Prog. Oceanogr.*, *139*, 171–196,
1016   doi:10.1016/j.pocean.2015.08.009.

1017   Trimble, S. M., and M. Baskaran (2005), The role of suspended particulate matter in 234Th
1018   scavenging and 234Th-derived export fluxes of POC in the Canada Basin of the Arctic
1019   Ocean, *Mar. Chem.*, *96*(1-2), 1–19, doi:10.1016/j.marchem.2004.10.003.

1020   Uitz, J., H. Claustre, A. Morel, and S. B. Hooker (2006), Vertical distribution of phytoplankton
1021   communities in open ocean: An assessment based on surface chlorophyll, *J. Geophys. Res.*
1022   *Ocean.*, *111*(C8), 23 pp., doi:10.1029/2005JC003207.

1023   Verdeny, E., P. Masqué, K. Maiti, J. Garcia-Orellana, J. M. Bruach, C. Mahaffey, and C. R.
1024   Benitez-Nelson (2008), Particle export within cyclonic Hawaiian lee eddies derived from
1025   210Pb–210Po disequilibrium, *Deep Sea Res. Part II Top. Stud. Oceanogr.*, *55*(10-13),
1026   1461–1472, doi:10.1016/j.dsr2.2008.02.009.

1027   Verdeny, E., P. Masqué, J. Garcia-Orellana, C. Hanfland, J. Kirk Cochran, and G. M. Stewart
1028   (2009), POC export from ocean surface waters by means of 234Th/238U and 210Po/210Pb
1029   disequilibria: A review of the use of two radiotracer pairs, *Deep Sea Res. Part II Top. Stud.*
1030   *Oceanogr.*, *56*(18), 1502–1518, doi:10.1016/j.dsr2.2008.12.018.

1031   Waite, A. M., K. A. Safi, J. A. Hall, and S. D. Nodder (2000), Mass sedimentation of
1032   picoplankton embedded in organic aggregates, *Limnol. Oceanogr.*, *45*(1), 87–97,
1033   doi:10.4319/lo.2000.45.1.0087.

1034   Wassmann, P. (2011), Arctic marine ecosystems in an era of rapid climate change, *Prog.*

Post print version of manuscript accepted for *Journal of Geophysical Research - Oceans*

1035   *Oceanogr.*, *90*(1-4), 1–17, doi:10.1016/j.pocean.2011.02.002.

1036 Wei, C.-L., S.-Y. Lin, D. D.-D. Sheu, W.-C. Chou, M.-C. Yi, P. H. Santschi, and L.-S. Wen
1037   (2011), Particle-reactive radionuclides (234Th, 210Pb, 210Po) as tracers for the estimation
1038   of export production in the South China Sea, *Biogeosciences*, *8*(12), 3793–3808,
1039   doi:10.5194/bg-8-3793-2011.

1040 Wilson, S., and D. K. Steinberg (2010), Autotrophic picoplankton in mesozooplankton guts:
1041   evidence of aggregate feeding in the mesopelagic zone and export of small phytoplankton,
1042   *Mar. Ecol. Prog. Ser.*, *412*, 11–27, doi:10.3354/meps08648.

1043 Yu, W., L. Chen, J. Cheng, J. He, M. Yin, and Z. Zeng (2010), 234Th-derived particulate
1044   organic carbon export flux in the western Arctic Ocean, *Chinese J. Oceanol. Limnol.*, *28*(6),
1045   1146–1151, doi:10.1007/s00343-010-9933-1.

1046 Yu, W., J. He, Y. Li, W. Lin, and L. Chen (2012), Particulate organic carbon export fluxes and
1047   validation of steady state model of 234Th export in the Chukchi Sea, *Deep Sea Res. Part II*
1048   *Top. Stud. Oceanogr.*, *81-84*, 63–71, doi:10.1016/j.dsr2.2012.03.003.

1049 Zhang, F., J. He, L. Lin, and H. Jin (2015), Dominance of picophytoplankton in the newly open
1050   surface water of the central Arctic Ocean, *Polar Biol.*, *38*(7), 1081–1089,
1051   doi:10.1007/s00300-015-1662-7.

1052

41